박사 학위논문

Ph. D. Dissertation

이방성 전도도를 복구하는 문제의 Well-posedness

Well-posedness in anisotropic conductivity reconstruction

이 민 기 (李 民 基 Lee, Min-Gi)

수리과학과

Department of Mathematical Sciences

KAIST

2014

이방성 전도도를 복구하는 문제의 Well-posedness

Well-posedness in anisotropic conductivity reconstruction

Well-posedness in anisotropic conductivity reconstruction

Advisor : Professor Kim, Yong-Jung

by

Lee, Min-Gi

Department of Mathematical Sciences

KAIST

A thesis submitted to the faculty of KAIST in partial fulfillment of the requirements for the degree of Doctor of Philosophy in the Department of Mathematical Sciences . The study was conducted in accordance with Code of Research Ethics[1].

2014. 5. 16.

Approved by

Professor Kim, Yong-Jung

[Advisor]

---

[1]Declaration of Ethical Conduct in Research: I, as a graduate student of KAIST, hereby declare that I have not committed any acts that may damage the credibility of my research. These include, but are not limited to: falsification, thesis written by someone else, distortion of research findings or plagiarism. I affirm that my thesis contains honest conclusions based on my own careful research under the guidance of my thesis advisor.

이방성 전도도를 복구하는 문제의 Well-posedness

이 민 기

위 논문은 한국과학기술원 박사학위논문으로
학위논문심사위원회에서 심사 통과하였음.

2014년 5월 16일

심사위원장 김 용 정 (인)

심사위원 변 재 형 (인)

심사위원 임 미 경 (인)

심사위원 강 현 배 (인)

심사위원 권 오 인 (인)

DMAS
20095345

이 민 기. Lee, Min-Gi. Well-posedness in anisotropic conductivity reconstruction. 이방성 전도도를 복구하는 문제의 Well-posedness. Department of Mathematical Sciences . 2014. 50p. Advisor Prof. Kim, Yong-Jung. Text in English.

ABSTRACT

In the thesis, interior conductivity reconstruction problems inferring from the interior current density data are considered. It is our main result that an anisotropic conductivity reconstruction in two dimensions is well-posed. This is relevant to an application of a medical diagnosis on human organism since human organism typically has an anisotropic conductivity.

In the first part of thesis, the well-posedness theorems on isotropic, orthotropic, and anisotropic conductivities are presented. An existence theorem is treated to the same extent as an uniqueness theorem; The admissibility conditions on the current data that are sufficient to imply the existence of the solution are defined prior to stating the theorems. They provide sufficient conditions to characterize differences between arbitrary vector fields and the current vector fields that are realizable electrically. The main results comes from that we can pose an equation or a system of equations of hyperbolic type on the solution.

In the second part of thesis, a numerical algorithm to reconstruct the conductivity is suggested. Isotropic and orthotropic materials can be treated by the algorithm. The algorithm has two advantages: Firstly, the conductivity reconstruction is obtained by directly solving equations of hyperbolic type without iteration process. Secondly, numerical approximations of divergence and curl operator are exact, which is known to be of mimetic type. Since this scheme is realized as a resistive network of circuit theory in our context, we call the algorithm Virtual Resistive Network algorithm. Propagation of noises and the stability of the algorithm is investigated. Due to the nature of the hyperbolic problems, the noises would propagate along characteristic lines without cancellation. The numerical scheme composed by the mimetic idea turns out to be the one that may relax the hyperbolic nature of noise propagation.

Contents

List of Tables

List of Figures

Chapter 1. Introduction

1.1 Introduction

This thesis is about the conductivity construction problem inferred from the interior current density data. The most important concept in this thesis is the *Ohm's Law* which states the existence of the linear relationship between the electric field and the current density field in the following form.

$$\mathbf{J} = \sigma \mathbf{E}.$$

The proportionality σ is called the conductivity at the point. This constitutive law is known to be good deal exact in a wide range of materials even in the nano scale.

The conductivity value is supposed to persist under the extent variance of the environment, in particular when the undergoing electro-magnetic phenomena is close to the static case. Then we could refer the value as the intrinsic property of the material. In such a case the conductivity can give or suggest information on the status of the material as in the cases we infer information from various other properties via X-ray, Ultrasound, CT, and etc.

The conductivity possibly changes both the magnitude and the direction of the loaded vector $\mathbf{E}$. The direction cannot be reversed however, more concretely, the change of the angle cannot exceed $\frac{\pi}{2}$. In d-dimensions, it is also assumed that there are d principal directions, orthogonal to each other, and d possibly distinct corresponding conductivity values such that an $\mathbf{E}$ in one of those directions becomes an eigenvector of the conductivity with the corresponding conductivity value as eigenvalue. Hence the conductivity is set as a symmetric and positive definite matrix for each point. As a special case, when all the d eigenvalues agree, i.e. when the conductivity matrix is a scalar multiple of identity matrix, it is said to be *isotropic*. The conductivity is *anisotropic* if it is not isotropic. For a given body occupying a region $\Omega \subset \mathbb{R}^d$, the conductivity is therefore the matrix field. If the conductivities in Ω is simultaneously diagonalizable, which is in general impossible, we call the field the *orthotropic* conductivity field. In such a case we may choose a coordinate system in which the field is the diagonal matrix field.

Once Ohm's Law is admitted, the overall electro-magneto-static phenomena in a given body Ω is determined by the following single equation

$$\nabla \cdot (\sigma \nabla u) = 0, \tag{1.1}$$

$$-\sigma \nabla u \cdot \mathbf{n} = g, \tag{1.2}$$

where u is a potential for the electric field so that $\mathbf{E} = -\nabla u$ and hence $\mathbf{J} = -\sigma \nabla u$. g is the normal component of current on $\partial\Omega$ controlled by for example electrodes attached to the body. g has to satisfy the condition

$$\int_{\partial\Omega} g = 0$$

in order the equation to be solved. Other fields such as magnetic field and charge distribution then are determined by the maxwell's system of equations.

The conductivity for each point can be determined by measuring at least d $\mathbf{J}$ vectors caused by d linearly independent $\mathbf{E}$ vectors at the point. This is in fact over-determined because the conductivity is

symmetric furthermore. In many cases however, one cannot directly contact the interior point as one cannot in X-ray, Ultrasound, CT, and etc.

One therefore seeks a quantity that is equivalent or sufficient in ability to determine the conductivity for all points of the domain. The inferring process is typically formulated as solving an *inverse problem*. One most classical such quantity is the *Dirichilet to Neumann* map, the DN map for brevity. It is a map corresponds the voltage profile on the $\partial\Omega$ to the normal component of the current profile on the $\partial\Omega$. It is well-defined because the equation (1.1) with respect to the boundary condition

$$u|_{\partial\Omega} = f \tag{1.3}$$

consists a well-posed problem. Hence there is the unique normal component of the current on $\partial\Omega$ for each voltage profile f. Equivalently, one may consider *Neumann to Dirichile* map, or ND map.

Studies to infer conductivity from the DN map has been studied since eighties and now it becomes classical. The related technique is known to be Electrical Impedance Tomography (EIT) in the literature. See [1], [2], and [3]. For a given domain $\Omega \subset \mathbb{R}^d$, it is well-known that, for instance as in [4], this map, which is a function of Ω and σ, has sufficient information to determine the interior isotropic conductivity when $d \geq 2$. It is also fact that one can generate infinitely many anisotropic conductivity fields whose DN map is identical to the one of a certain isotropic conductivity field. In other words, DN map does not have a resolution to distinguish anisotropic conductivity fields.

The one we infer information from in this thesis is the interior current density. Questions how one measures such data without destructing the body is referred to papers concerning techniques of MRCDI, [5] and [6]. The purpose of this thesis is to give mathematical background for the theory. The related technique is known to be Magnetic Resonance Electrical Impedance Tomography (MREIT). See [7], [8], [9], [10], [11], [12], [13], [14], [15], [16], [17], [18], [19], [20],[21], [22], [23], and [24]. Other problems that make use of internal measurements are [25], [26], [27], [28], [29], and [30].

Main theme we can see in the thesis is the *powerfullness* of making use of interior data, which appears in the following formal statements we are going to advance.

1. Three current density data determine anisotropic conductivity uniquely.

2. Furthermore, the information is exact such that the problem is neither under-determined nor over-determined so that we can *construct* the one solution for the data.

3. The construction process is undergone by the solving a single or a system of partial differential equations of hyperbolic type according to the type of the conductivity we are assuming, in which we are saying that it is not a case of typical inverse problem. Since a hyperbolic partial differential equation is solved stably under the changes of initial-boundary data and the coefficients, and they come from the current density data, the conductivity is constructed stably for the given data.

In other words, we are stating that our concerned problem is well-posed.

The thesis consists mainly of two parts. In the following chapter, we present the theorems stating partial of full well-posedness of the construction problem with respect to isotropic, orthotropic, and anisotropic conductivity field. The other chapter is devoted to the study of numerical algorithm which we referes to as the *Virtual Resistive Network* algorithm. It constructs isotropic and orthotropic conductivity from discretely sampled current data.

Before we close this section, we specify one particular interpretation of the study. Sometimes the conductivity problem is connected to the purely mathematical questions in Riemannian geometry. This

is due to the fact that the Laplace-Beltrami operator in a Riemannian manifold with a metric g reads

$$\sum_{i,j=1}^{d} \frac{1}{\sqrt{|g|}} \partial_i (\sqrt{|g|} g^{ij} \partial_j u) = 0,$$

where the conductivity does a role as a $\sqrt{|g|}g^{ij}$ in the equation (1.1) of a same structure. Here $|g|$ is the determinant of g, and g^{ij} is an ij entry of g^{-1}. More concretely, $\sqrt{|g|}g^{ij}$ originates from the Hodge-star operation $*$ on a 1-form,

$$* \, (E_j \; dx^j) = \epsilon_{k_1,k_2,\ldots,k_{d-1},i} \sqrt{|g|} g^{ij} E_j \;\; dx^{k_1} \wedge dx^{k_1} \wedge \ldots \wedge dx^{k_{d-1}},$$

where $\epsilon_{k_1,k_2,\ldots,k_{d-1},i}$ is the d-dimensional Levi-Civita symbol. Thus the multiplication of the conductivity is the Levi-Civita detached Hodge-star operation. The Ohm's Law in this interpretation can be reads,

$$\omega_J = * \, \omega_E,$$

where $(\omega_J)_{k_1,k_2,\ldots,k_{d-1}} = \epsilon_{k_1,k_2,\ldots,k_{d-1},i} J^i$, and $(\omega_E)_j = E^j$, and J^j and E^j are the components of $\mathbf{J}$ and $\mathbf{E}$. ω_E becomes a harmonic 1-form and ω_J becomes a harmonic $(d-1)$-form due to the governing equation (1.1) and maxwell's equations.

Suppose we declare the several $(d-1)$-forms to be harmonic. Then one can ask whether there is a metric g by which the $(d-1)$-forms are indeed harmonic. We will present a partially positive answer when $d = 2$ in this thesis.

1.2 Ohm's Law and Irrotationality of Electric Field

Let us begin with emphasizing an importance of the equation (1.1), the incompressibility of $\mathbf{J}$ combined by Ohm's Law. Together with a boundary condition (1.2) or (1.3), the equation has the unique solution u, and consequently $\mathbf{E}$ and $\mathbf{J}$ are determined. From $\mathbf{E}$ and $\mathbf{J}$, other quantities describing the whole electro-magneto-static phenomena are fixed in principle by maxwell's equations (See Appendix for a list of quantities in maxwell's equations). For example, two of maxwell's equations are

$$\begin{aligned} \nabla \times \mathbf{H} &= \mathbf{J} \quad \text{in } \Omega, \\ \nabla \cdot (\mu \mathbf{H}) &= 0 \quad \text{in } \Omega, \end{aligned}$$

where μ is the permeability, and $\mathbf{H}$ is determined with an appropriate boundary condition. We may also fix the displacement field $\mathbf{D}$, the charge distribution ρ_f under supplements of appropriate information. In summary, the equation (1.1) the incompressibility of $\mathbf{J}$ combined by Ohm's Law is the very core of the whole phenomena, which is an equation of what we call the *forward problem*. Our *inverse problem* is the one relevant to that forward problem.

At this point, let us look up a work of Richter [26], which considered a kind of an inverse problem for isotropic conductivity from the information of interior potential u. His original work in fact concerned a more general situation and motivated from other context, but let us apply the result for our simpler case and keep using electro-magnetic terminology. If the equation (1.1) is expanded in two dimensions, since σ is isotropic we obtain

$$\big(\partial_x u\big)\partial_x \sigma + \big(\partial_y u\big)\partial_y \sigma + \big(\partial_x^2 u + \partial_y^2 u\big)\sigma = 0. \tag{1.4}$$

Expressions in parenthesis are known coefficients here to solve above equation for σ. The above is an linear first order equation and is solvable on where the method of characteristic is applicable.

Now let us return to our problem making use of $\mathbf{J}$, not $\mathbf{E}$. One immediately realizes that the incompressibility of $\mathbf{J}$ does not anymore supply an equation for σ, but it is a necessary condition for a given data. Until 2002 therefore, an iterative structure to solve the inverse problem was studied. The equation (1.1) to solve for u and the Ohm's Law to calculate $\mathbf{J}$ from it are alternatively used in each iteration in the following way. First, an ansatz for the conductivity is specified. Then, one solves (1.1) with the ansatz for $\mathbf{E}$ and $\mathbf{J}$. The resulted current would be different from the measured data, and one devise an algorithm to update the conductivity ansatz from that inconsistency. This procedure is iterated.

Comparing to the problem of Richter, this procedure is severely non-linear and is hardly analyzable mathematically; the non-linearity is to invert an elliptic operator in every iteration.

Now consider the Ohm's Law in a form of $\mathbf{E} = r\mathbf{J}$. $r = \sigma^{-1}$ is the *resistivity*. We consider in this thesis only an invertible conductivity. Then, one may consider an equation of

$$0 = \nabla \times \big(r\mathbf{J}\big) = (J^y)\partial_x r + (-J^x)\partial_y r + (\partial_x J^y - \partial_y J^x)r. \tag{1.5}$$

Observe that r is solvable by method of characteristic with a single $\mathbf{J}$ datum, similarly as done in the Richter's problem. Ider *et. al.* [15] and Lee [18] found the *identity* (1.5) useful in devising their algorithms. In fact, they made use of two current density data.

What we are trying to do here is to set up a new suitable framework. $\nabla \times \big(r\mathbf{J}\big) = 0$ is more than the useful identity; it takes its role in the whole electro-magneto-static phenomena as equivalent as (1.1) does. As a consequence of this criticality, throughout this thesis we are going to define our *forward problem* as following elliptic system.

$$\nabla \times \big(r\mathbf{J}\big) = 0 \quad \text{in } \Omega, \tag{1.6}$$

$$\nabla \cdot \mathbf{J} = 0 \quad \text{in } \Omega, \tag{1.7}$$

with a Neumann boundary condition

$$\mathbf{J} \cdot \mathbf{n} = g \quad \text{on } \partial\Omega. \tag{1.8}$$

or a Dirichilet boundary condition

$$r\mathbf{J} \cdot \mathbf{T} = f \quad \text{on } \partial\Omega. \tag{1.9}$$

This system is well-posed and thus it determines $\mathbf{J}$ and $\mathbf{E}$ uniquely. Equivalence in abilities to (1.1) follows from this fact and the earlier discussions in this section. Note that it is emphasized in the system that the electric field in a form combined by Ohm's Law is irrotational, and what appeared explicitly in the Ohm's Law is the resistivity rather than conductivity.

In summary, this thesis is about an inverse problem to construct the resistivity that is relevant to a forward problem (1.6)-(1.9).

Chapter 2. Well-posedness of Resistivity Construction Problem

2.1 Preliminaries

In this section, we collected what are shared in the analysis of this chapter. They are not the author's original work but they can be found in the literature.

$\mathbf{\Omega} \subset \mathbb{R}^2$ is a simply connected bounded domain with smooth boundary. Let $\mathbf{J}$ be a smooth vector field defined in $\bar{\Omega}$. If $\nabla \cdot \mathbf{J} = 0$ throughout the domain, we define a stream function ψ of $\mathbf{J}$ such that

$$\mathbf{J} = \begin{pmatrix} \partial_y \psi \\ -\partial_x \psi \end{pmatrix}.$$

The stream function is unique up to an addition of a constant.

Correspondingly, if $\mathbf{E}$ is a smooth vector field in $\bar{\Omega}$ such that $\nabla \times \mathbf{E} = 0$, we define a potential u such that

$$\mathbf{E} = -\nabla u.$$

We may express Ohm's Law as

$$\begin{pmatrix} \psi_y \\ -\psi_x \end{pmatrix} = -\sigma \begin{pmatrix} u_x \\ u_y \end{pmatrix}, \quad \text{or} \quad r \begin{pmatrix} \psi_y \\ -\psi_x \end{pmatrix} = - \begin{pmatrix} u_x \\ u_y \end{pmatrix}, \tag{2.1}$$

in which the irrotationality of $\mathbf{E}$ and the incompressibility of $\mathbf{J}$ are built-in.

Now for a given Neumann boundary condition g, the potential u is a solution of an elliptic equation

$$\begin{aligned} \nabla \cdot (\sigma \nabla u) &= 0, \quad \text{in } \Omega, \\ -\sigma \nabla u \cdot \mathbf{n} &= g, \quad \text{on } \partial\Omega. \end{aligned}$$

The current field $\mathbf{J}$ and its stream function ψ is related by (2.1). From

$$r \begin{pmatrix} \psi_y \\ -\psi_x \end{pmatrix} = r \begin{pmatrix} 0 & 1 \\ -1 & 0 \end{pmatrix} \begin{pmatrix} \psi_x \\ \psi_y \end{pmatrix}, \quad - \begin{pmatrix} u_x \\ u_y \end{pmatrix} = - \begin{pmatrix} 0 & -1 \\ 1 & 0 \end{pmatrix} \begin{pmatrix} u_y \\ -u_x \end{pmatrix},$$

we may write

$$\begin{pmatrix} u_y \\ -u_x \end{pmatrix} = \begin{pmatrix} 0 & -1 \\ 1 & 0 \end{pmatrix} r \begin{pmatrix} 0 & 1 \\ -1 & 0 \end{pmatrix} \begin{pmatrix} \psi_x \\ \psi_y \end{pmatrix} = s \begin{pmatrix} \psi_x \\ \psi_y \end{pmatrix},$$

where $s := \begin{pmatrix} 0 & -1 \\ 1 & 0 \end{pmatrix} r \begin{pmatrix} 0 & 1 \\ -1 & 0 \end{pmatrix}$. It is also a symmetric positive definite matrix field. Observe that the left-hand-side is divergence-free. Hence

$$0 = \nabla \cdot (s \begin{pmatrix} \psi_x \\ \psi_y \end{pmatrix})$$

We may also check that

$$0 = \nabla \cdot (s \begin{pmatrix} \psi_x \\ \psi_y \end{pmatrix}) = \nabla \times (r \begin{pmatrix} \psi_y \\ -\psi_x \end{pmatrix}).$$

The boundary condition

$$g = -\sigma \nabla u \cdot \mathbf{n} = (\psi_y, -\psi_x) \cdot (n_1, n_2) = (\psi_x, \psi_y) \cdot (-n_2, n_1) = \nabla \psi \cdot T,$$

where T is a unit tangent vector along the boundary counter-clockwisely. Define $\gamma(\ell) : [0, L] \mapsto \partial\Omega$, an embedding from an arc-length parameter ℓ to the boundary $\partial\Omega$, where L is a total length of $\partial\Omega$. Then one can integrate the $\nabla\psi \cdot T = \psi'(\gamma(\ell))$ to have

$$\psi(\gamma(\ell)) = G(\gamma(\ell)) := \int_0^\ell g\big(\gamma(\ell')\big) d\ell'.$$

Since an addition of a constant to the ψ does not change physics at all, we fixed $\psi(\gamma(0)) = 0$ in the formula.

Hence if u is a solution of an elliptic equation with a Neumann boundary condition g, then the induced stream function ψ is a solution of an associated elliptic equation with Dirichilet boundary condition G as below.

$$\nabla \cdot (s \nabla \psi) = 0, \quad \text{in } \Omega, \tag{2.2}$$

$$\psi = G, \quad \text{on } \partial\Omega. \tag{2.3}$$

In conclusion, the first order system (1.6)-(1.8) reduces to a single divergence type second order equation (2.2)-(2.3) in two dimensions.

Remark 2.1.1. *Note that in the* (2.2)-(2.3)*, the stream function ψ appears as if it is a potential. Hence for the isotropic conductivity in two dimensions, this problem reduces to the problem of Richter [26] that makes use of a potential datum.*

Now, we list a formula under a change of coordinate system. Suppose (ξ, η) is an another coordinate chart on the domain. From chain rule,

$$r \begin{pmatrix} \psi_y \\ -\psi_x \end{pmatrix} = r \begin{pmatrix} \eta_y & -\xi_y \\ -\eta_x & \xi_x \end{pmatrix} \begin{pmatrix} \psi_\eta \\ -\psi_\xi \end{pmatrix}, \quad - \begin{pmatrix} u_x \\ u_y \end{pmatrix} = - \begin{pmatrix} \xi_x & \eta_x \\ \xi_y & \eta_y \end{pmatrix} \begin{pmatrix} u_\xi \\ u_\eta \end{pmatrix},$$

and from Ohm's Law

$$\frac{1}{\xi_x \eta_y - \eta_x \xi_y} \begin{pmatrix} \eta_y & -\eta_x \\ -\xi_y & \xi_x \end{pmatrix} r \begin{pmatrix} \eta_y & -\xi_y \\ -\eta_x & \xi_x \end{pmatrix} \begin{pmatrix} \psi_\eta \\ -\psi_\xi \end{pmatrix} = - \begin{pmatrix} u_\xi \\ u_\eta \end{pmatrix}.$$

Define $R := \frac{1}{\xi_x \eta_y - \eta_x \xi_y} \begin{pmatrix} \eta_y & -\eta_x \\ -\xi_y & \xi_x \end{pmatrix} r \begin{pmatrix} \eta_y & -\xi_y \\ -\eta_x & \xi_x \end{pmatrix}$, then R is a symmetric positive definite matrix field and we have a version of an Ohm's Law

$$R \begin{pmatrix} \psi_\eta \\ -\psi_\xi \end{pmatrix} = - \begin{pmatrix} u_\xi \\ u_\eta \end{pmatrix} \tag{2.4}$$

in the (ξ, η) coordinate system. We may further define $S := \begin{pmatrix} 0 & -1 \\ 1 & 0 \end{pmatrix} R \begin{pmatrix} 0 & 1 \\ -1 & 0 \end{pmatrix}$ similarly as before. Note that one of σ, r, s, R, and S fixes remainders, so we may construct one of them.

Lastly, the following is a result in [31] that is frequently cited in this thesis.

Lemma 2.1.1 (Alessandrini, 1987)**.** *Let $a_{ij} \in C^1(\Omega)$, $b_i \in C(\Omega)$, $i,j = 1,2$ and let $g \in C(\bar{\Omega})$. Let $u \in W^2_{loc}(\Omega) \cap C(\bar{\Omega})$ satisfy*

$$\sum_{i,j=1}^{2} a_{ij} u_{x_i x_j} + \sum_{i=1}^{2} b_i u_{x_i} = 0, \quad \text{in } \Omega,$$

$$u = g, \quad \text{on } \partial\Omega.$$

$\Omega \subset \mathbb{R}^2$ is a bounded simply connected domain.

If $g|_{\partial\Omega}$ has N maxima (and N minima), then the interior critical points of u are finite in number and, denoting by $m_1, \cdots, m_K$ their multiplicities, the following estimate holds

$$\sum_{i=1}^{K} m_i \leq N - 1.$$

2.2 Well-posedness of Isotropic Resistivity Construction Problem

In this section, we try to solve a following partial differential equation

$$\begin{aligned} \nabla \times \big(r\mathbf{F}\big) = 0, \quad &\text{in } \Omega, \\ r = r_0, \quad &\text{on } \Gamma \subset \partial\Omega. \end{aligned} \tag{2.5}$$

for a real-valued function $r : \bar{\Omega} \mapsto \mathbb{R}^+$, with respect to the coefficients $\mathbf{F}$ and an initial condition r_0 defined on a portion Γ of the boundary. We denoted the vector field by $\mathbf{F}$ instead of $\mathbf{J}$ to give a certain generality to the datum.

As discussed earlier, this linear equation is solved by the method of characteristic. Resistivity on where is covered by characteristic lines emanating from the Γ, will be determined by the method. Here, we want this process to be precise: we are going to define a condition on the datum and the initial surface Γ so that the family of characteristic lines behave nicely enough so that we determine the resistivity on $\bar{\Omega}$ exactly. On the while, we relax the condition on the datum as much as it could be.

Let us first examine that from what kind of datum we may construct a physically meaningful resistivity. Noise possibly breaks the divergence-free condition for example, or $\nabla \cdot \mathbf{F} = h$. This is indeed the cases we encounter in practice, but the existence is hardly questioned. We cover the case as the one when there is an internal source h.

Recall that our problem has an interpretation to find a metric after declaring a certain field to be harmonic. In two dimensional case, the stream function ψ is declared to be harmonic, i.e. it is a solution of an equation of Laplace-Beltrami. It is obvious that arbitrary stream function cannot be the one, it cannot have interior maxima and minima because of maximum principle, and cannot be a constant in an open set because of the Unique Continuation Property for instances.

On the other hand, if a stream function, or $\mathbf{F}$, is generated from a given resistivity, then there necessarily exists a solution for the datum. However, it is a different issue whether the family of characteristic lines defined from the one has sufficient resolution to recover the information.

2.2.1 Admissibility of Datum

Motivated from preceding discussions, let us define an admissibility as follows.

Definition 2.2.1 (Admissibiliy 1)**.** *Consider a two dimensional vector field $\mathbf{F} = (f^1, f^2) \in C^{1,\alpha}(\bar{\Omega})$ for $0 < \alpha < 1$. Denote $\Gamma^+ := \{\mathbf{x} \in \partial\Omega \,|\, \mathbf{F}^\perp \cdot \mathbf{n}(\mathbf{x}) > 0\}$, $\Gamma^- := \{\mathbf{x} \in \partial\Omega \,|\, \mathbf{F}^\perp \cdot \mathbf{n}(\mathbf{x}) < 0\}$, $\Gamma^0 := \{\mathbf{x} \in \partial\Omega \,|\, \mathbf{F}^\perp \cdot \mathbf{n}(\mathbf{x}) = 0\}$, where $\mathbf{F}^\perp := (-f^2, f^1)$. The vector field $\mathbf{F}$ is called admissible in this section if $\mathbf{F} \neq 0$ in $\bar{\Omega}$ and $\Gamma^\pm$ are connected. Also Γ^- is called an admissible boundary.*

The geometry of boundary is illustrated in the Figure 2.1(a). We are are excluding cases for example the one in Figure 2.1(b), where Γ^- has several connected components. Both of them are actually realizable electrically. Let us explain the consequence of the connectedness of Γ^-. Suppose σ has a jump discontinuity. Then in general it is detected by $\mathbf{F}$ by the jump of the tangential component of the current $\mathbf{F}$ along the discontinuity. If the discontinuity occurs along an equipotential line, where the tangential component of $\mathbf{F}$ vanishes, it is not detected by $\mathbf{F}$. However, it can be proved that the very equipotential line has to intersect a boundary. If the intersection point is in the interior of Γ^-, then the jump discontinuity is detected by the jump of initial data r_0. Even when r_0 does not have a jump, if r_0

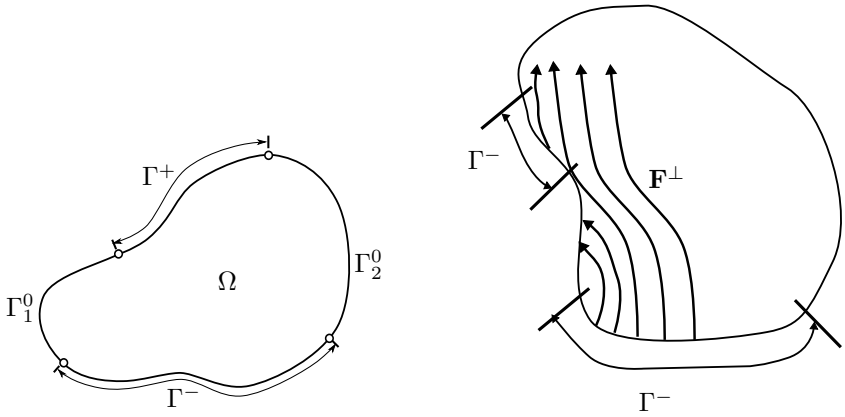

(a) Admissible boundary (b) Not an admissible boundary

Figure 2.1: Domain Boundary: The boundary of the domain is divided into four parts depending on the given admissible vector field $\mathbf{F}$ in the sense of Definition 2.2.1.

is defined on several disjoint sets, it is allowed to have a jump discontinuity along the equipotential line emanating from boundary between the sets. In short, if Γ^- has only one connected component, then the jump discontinuity has to cause the jump in either $\mathbf{F}$ or r_0. Hence the admissible datum is the one that is well-designed to recover information on conductivity, and is more than the one that is realizable.

In the end of this section, we contained a theorem stating that the condition is achievable only by controlling a boundary condition. This is a consequence of Lemma 2.1.1 of Alessandrini, and the proof can be found in the literature, for example in Nachman *et. al.* [19]. For a completeness we provided the proof.

Now we investigate the consequences of the admissibility. Let $\mathcal{C}$ be a family of integral curves of the vector field $\mathbf{F}^\perp$. The integral curve extended from $\mathbf{x}_0$ is a solution of the ordinary differential equation (or ODE for brevity)

$$\frac{d}{dt}\mathbf{x}(t) = F^\perp(\mathbf{x}(t)), \quad \mathbf{x}(0) = \mathbf{x}_0, \quad -\infty < t < \infty. \tag{2.6}$$

In the following lemma we quickly summarize elementary properties of integral curves of a non-vanishing C^1 vector field in a compact domain $\bar{\Omega}$.

Lemma 2.2.1. *If $X \in C^1(\bar{\Omega})$ and $X \neq 0$ in $\bar{\Omega}$, then*

(i) Integral curves of X do not touch other ones nor themselves.

(ii) The length of an integral curves of X is uniformly bounded.

(iii) Both ends of an integral curve of X are extendable to the boundary.

Proof. Let $\mathbf{x}_0$ be a tangential or intersection point of two different integral curves. This implies that there exist two solutions of (2.6) locally at $\mathbf{x}_0$. However, X is assumed to be C^1 and hence it contradicts to existence of unique solutions to such ODEs and hence we obtained the first assertion.

The second assertion depends on the assumption $X \neq 0$ in $\bar{\Omega}$. Suppose that there is an integral curve $\mathbf{x}(t)$ which is infinitely long. Then, since the domain Ω is bounded, there exist nonempty limit set $\omega(\mathbf{x})$. Since there is no critical point, Poincare-Bendixon implies that $\omega(\mathbf{x})$ is a periodic orbit. This implies that there exists a critical point in the interior of the orbit, which contradicts to the assumption $X \neq 0$ in $\bar{\Omega}$. Therefore, all the integral curves are finitely long. Since $\bar{\Omega}$ is compact, they are uniformly bounded.

Since $\bar{\Omega}$ is compact and $|X| > 0$ on $\bar{\Omega}$, there exists a lower bound $a > 0$ such that

$$|X| \geq a > 0.$$

Suppose that an integral curve $\mathbf{x}(t)$ converges to an interior point $\mathbf{y} \in \Omega$ as $t \to \infty$. One can easily see that this is not possible since the speed of the curve is uniformly bounded from below, i.e., $|\mathbf{x}'(t)| = |X(\mathbf{x}(t)| \geq a$, the curve cannot stay in a small neighborhood of $\mathbf{y}$ forever. Therefore, the integral curve $\mathbf{x}$ should connect two boundary points of $\partial\Omega$. □

In the following lemma, the connectedness of Γ^- implies that all the integral curves should connect the boundaries Γ^- and Γ^+.

Lemma 2.2.2. *If $\mathbf{F}$ is admissible, then the integral curve of $\mathbf{F}^\perp$ that passes through an interior point $\mathbf{x}_0 \in \Omega$ starts from Γ^- and ends at Γ^+. There exists $T > 0$ a uniform upper bound of the domain size of integral curves.*

Proof. Since the vector field $\mathbf{F}$ is assumed to be admissible, the boundary $\partial\Omega$ is divided into four parts, $\partial\Omega = \Gamma^- \cup \Gamma_1^0 \cup \Gamma^+ \cup \Gamma_2^0$, where $\mathbf{F}^\perp \cdot \mathbf{n}(\mathbf{x}) = 0$ on Γ_i^0 (see Figure 2.1).

Note that each Γ_i^0 is a single point or is an integral curve of $\mathbf{F}^\perp$ by definition. From Lemma 2.2.1, we know that the integral curve that passes through an interior point $\mathbf{x}_0$ is unique and has two end points on $\partial\Omega$, i.e., there exist $t_- < 0 < t_+$ such that

$$\mathbf{x}'(t) = \mathbf{F}^\perp(\mathbf{x}(t)) \quad \text{for} \quad t_- < t < t_+, \quad \mathbf{x}(t_-), \mathbf{x}(t_+) \in \partial\Omega.$$

Since $\mathbf{x}'(t_-) \cdot \mathbf{n} \leq 0$ and $\mathbf{x}'(t_+) \cdot \mathbf{n} \geq 0$, we have $\mathbf{x}(t_-) \in \Gamma^- \cup \Gamma_1^0 \cup \Gamma_2^0$ and $\mathbf{x}(t_+) \in \Gamma^+ \cup \Gamma_1^0 \cup \Gamma_2^0$. If any of Γ_i^0's is not a single point, then they are integral curves by definition. Since two integral curves do not intersect with each other by Lemma 2.2.1, we can conclude $\mathbf{x}(t_-) \in \Gamma^-$ and $\mathbf{x}(t_+) \in \Gamma^+$ and first part of proof is done.

Suppose that Γ_1^0 is a single point and $\mathbf{x}(t_-) \in \Gamma_1^0$ as in Figure 2.2. Then, $\mathbf{x}(t_+) \in \Gamma^+ \cup \Gamma_2^0$. If Γ_2^0 is not an single point, then, by the same reason, $\mathbf{x}(t_+) \in \Gamma^+$. In any case, $\mathbf{x}(t_+) \in \bar{\Gamma}^+ \setminus \Gamma_1^0$. Let $\mathbf{y}_0$ be an interior point of a region surrounded by the integral curve $\mathbf{x}(t)$, $t_- < t < t_+$, and Γ^+. The integral curve $\mathbf{y}(t)$ that passes through the point $\mathbf{y}_0$ should start from $\bar{\Gamma}^-$. Therefore, the integral curve $\mathbf{y}(t)$ should intersect the integral curve $\mathbf{x}(t)$, which contradicts to Lemma 2.2.1. Therefore $\mathbf{x}(t_-) \notin \Gamma_1^0$ even if Γ_1^0 is a single point. Similarly $\mathbf{x}(t_-) \notin \Gamma_2^0$ and hence $\mathbf{x}(t_-) \in \Gamma^-$. The same arguments also gives $\mathbf{x}(t_+) \in \Gamma^+$ and the first part of proof is complete.

Since the $|\mathbf{F}^\perp|$ is uniformly bounded below away from zero and the length of an integral curve is uniformly bounded, there exists $T > 0$ such that the domain size of any integral curve is less than T, i.e.,

$$t_+ - t_- \leq T,$$

which completes the proof □

We will always consider an admissible vector field in Definition 2.2.1. The boundary Γ^- is assumed to be smooth, where the curve $\gamma : [0, L] \to \bar{\Gamma}^-$ is $C^{2,\alpha}$. We will write the whole set of integral curves appeared earlier into a mapping of two parameters, such that

$$\frac{\partial}{\partial t}\mathbf{x}(s,t) = \mathbf{F}^\perp(\mathbf{x}(s,t)), \quad \mathbf{x}(s,0) = \gamma(s), \quad 0 \leq s \leq L. \tag{2.7}$$

The domain of the mapping $\mathbf{x}$ is a the closure of a bounded open subset $E \subset [0, L] \times [0, T]$. In the following lemma we will see that the mapping $\mathbf{x}$ gives a new coordinate system of the problem.

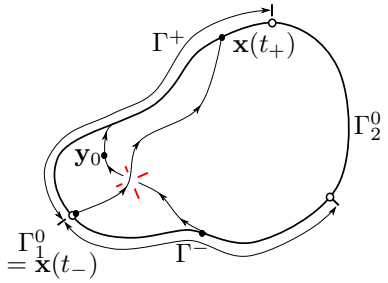

Figure 2.2: An illustration for the proof of Lemma 2.2.2.

Lemma 2.2.3. *Let* $\mathbf{F}$ *be admissible. Denote* $\Omega' := \bar{\Omega} \setminus \Gamma^0$. *(i) The mapping* $\mathbf{x} : \bar{E} \to \bar{\Omega}$ *defined by the relation* (2.7) *is a homeomorphism. (ii) Furthermore, its restriction* $\mathbf{x} : E' \to \Omega'$ *is a* C^1*-diffeomorphism, where* $E' = \mathbf{x}^{-1}(\Omega')$.

Proof. Lemma 2.2.1 implies that the mapping $\mathbf{x} : \bar{E} \to \bar{\Omega}$ is one-to-one. If not, $\mathbf{x}(s,t) = \mathbf{x}(s',t')$ for some $(s,t) \neq (s',t')$. This implies that an integral curve is touched by another one, if $s \neq s'$, or by itself, if $s = s'$. Then, it is against Lemma 2.2.1(i). Lemma 2.2.2 implies that $\Omega' \subset \mathbf{x}(\bar{E})$. To show $\mathbf{x}$ is a surjection, it is enough to show that Γ_1^0 and Γ_2^0 are actually integral curves $\mathbf{x}(0,\cdot)$ and $\mathbf{x}(L,\cdot)$. If each of them is a single point, then we do not need to be bothered. If not, we already know from Definition 2.2.1 that they are.

Now we show that $\mathbf{x}$ is continuous. In fact we will show that it is Lipschitz. Consider

$$|\mathbf{x}(s,t) - \mathbf{x}(s',t')| \leq |\mathbf{x}(s,t) - \mathbf{x}(s,t')| + |\mathbf{x}(s,t') - \mathbf{x}(s',t')|.$$

The first term is estimated by

$$|\mathbf{x}(s,t) - \mathbf{x}(s,t')| \leq \|\partial_t \mathbf{x}\|_\infty |t - t'| \leq \|\mathbf{F}\|_\infty \, |t - t'|.$$

To estimate the second term, we first consider

$$\begin{aligned} \frac{\partial}{\partial t}|\mathbf{x}(s,t) - \mathbf{x}(s',t)|\Big|_{t=t'} &= |\mathbf{F}^\perp(\mathbf{x}(s,t')) - \mathbf{F}^\perp(\mathbf{x}(s',t'))| \\ &\leq \|D\mathbf{F}\|_\infty \, |\mathbf{x}(s,t') - \mathbf{x}(s',t')|. \end{aligned}$$

Therefore, Gronwall's inequality gives, for $C = e^{T\|D\mathbf{F}\|_\infty}$,

$$\begin{aligned} |\mathbf{x}(s,t) - \mathbf{x}(s',t)| \quad &\leq C|\mathbf{x}(s,0) - \mathbf{x}(s',0)| \\ &= C|\gamma(s) - \gamma(s')| \\ &\leq C \, \|\gamma'\|_\infty \, |s - s'|. \end{aligned}$$

Combining these estimates, we have, for some constant $C > 0$,

$$|\mathbf{x}(s,t) - \mathbf{x}(s',t')| \leq C|(s,t) - (s',t')|. \tag{2.8}$$

Furthermore, since $\mathbf{x}$ is a continuous bijection from a compact set to a compact set, its inverse is also continuous and hence $\mathbf{x}$ is homeomorphism.

Differentiability of the mapping $\mathbf{x}(s,t)$ in s and t variables in E' is well-known from ODE theory (see Theorem 7.5 in [32] on pp.30 and remark on pp.23). We now show the differentiability of $\mathbf{x}^{-1}$ on

Ω'. To do that it is enough to show that the determinant of the Jacobian matrix $D\mathbf{x}(s,t)$ is not zero on E'. Differentiating (2.7) with respect to t and s gives

$$\partial_t \partial_s \mathbf{x}(s,t) = D\mathbf{F}^{\perp}(\mathbf{x}(s,t))\partial_s \mathbf{x}(s,t),$$
$$\partial_t \partial_t \mathbf{x}(s,t) = D\mathbf{F}^{\perp}(\mathbf{x}(s,t))\partial_t \mathbf{x}(s,t),$$

which can be written in terms of Jacobian matrix as

$$\partial_t D\mathbf{x}(s,t) = D\mathbf{F}^{\perp}(\mathbf{x}(s,t))D\mathbf{x}(s,t).$$

Therefore, the determinant of the Jacobian matrix is given by

$$\big|D\mathbf{x}(s,t)\big| = \big|D\mathbf{x}(s,0)\big| \exp\Big(\int_0^t tr\big(D\mathbf{F}^{\perp}(\mathbf{x}(s,\tau))\big)\, d\tau\Big),$$

(see Thoerem 7.3 in [32], pp28). On the other hand,

$$\big|D\mathbf{x}(s,0)\big| = \big|[\partial_s \mathbf{x}(s,0), \partial_t \mathbf{x}(s,0)]\big| = \gamma'(s) \times \mathbf{F}^{\perp}(\gamma(s)).$$

Since $\mathbf{F}^{\perp}(\gamma(s)) \cdot \mathbf{n} < 0$ for $\gamma(s) \in \Gamma^-$ and $\gamma'(s) \cdot \mathbf{n} = 0$, $\mathbf{F}^{\perp}(\gamma(s))$ and $\gamma'(s)$ are not parallel to each other. Therefore, $\big|D\mathbf{x}(s,0)\big| \neq 0$ and hence $\big|D\mathbf{x}(s,t)\big| \neq 0$ for all $t > 0$ for all $(s,t) \in E'$. □

Theorem 1. *Suppose the conductivity $\sigma \in C^{1,\alpha}(\bar{\Omega})$, a symmetric positive definite matrix field is given. Then there is a choice of Dirichilet boundary conditions f, such that $\mathbf{J} = -\sigma\nabla u$ is admissible, where u is a solution of an elliptic equation*

$$\nabla \cdot (\sigma \nabla u) = 0, \quad \text{in } \Omega,$$
$$u = f, \quad \text{on } \partial\Omega.$$

Proof. The proof can be found in [19]. Let $\gamma(\ell)$ be the embedding of $\partial\Omega$ as before. Choose $f(\gamma(\ell))$ that is strictly monotone except on the unique maximum and minimum. Then by 2.1.1, $\nabla u \neq 0$ in the interior and hence $\mathbf{J} \neq 0$ in the interior. The only points where u attains maximum and minimum are the possible critical points, but by Hopf's Lemma, $\nabla u \cdot \mathbf{n} \neq 0$ at there. Since $\mathbf{J}^{\perp} \cdot \mathbf{n} = (-J^1, J^2) \cdot (n_1, n_2) = (J^1, J^2) \cdot (-n_2, n_1) = -\sigma\nabla u \cdot T$, Γ^- is where $u(\gamma(\ell))$ is strictly increasing. By the definition of f, it has only one connected component. □

2.2.2 Main theorem

Now we are ready to prove our main result on the isotropic conductivity through the following theorem.

Theorem 2. *Let Ω be a bounded simply connected open set with $C^{2,\alpha}$ boundary. Suppose that an admissible vector field $\mathbf{F} \in C^{1,\alpha}(\bar{\Omega})$ and a boundary resistivity $r_0 \in C^{0,\alpha}(\bar{\Gamma}^-)$ are given. Then,*

(i) There exists a unique $r \in C^{0,\alpha}_{loc}(\Omega') \cap C^0(\bar{\Omega})$ that satisfies (2.5).

(ii) Let $\tilde{r}$ be the solution for an admissible vector field $\tilde{\mathbf{F}}$ with $\tilde{\Gamma}^- = \Gamma^-$ and a $\tilde{r}_0 \in C^{0,\alpha}(\bar{\Gamma}^-)$. Then,

$$\|r - \tilde{r}\|_{L^\infty(\bar{\Omega})} \leq C\left(\|r_0 - \tilde{r}_0\|_{L^\infty(\Gamma^-)} + \|\mathbf{F} - \tilde{\mathbf{F}}\|_{C^1(\bar{\Omega})}\right) + \omega\Big(\|\mathbf{F} - \tilde{\mathbf{F}}\|_{L^\infty(\bar{\Omega})}\Big), \tag{2.9}$$

where $C = C\big(\|F\|_{C^{1,\alpha}(\bar{\Omega})}, \|\tilde{F}\|_{C^{1,\alpha}(\bar{\Omega})}, \|r_0\|_{C^{0,\alpha}(\bar{\Omega})}, \|\tilde{r}_0\|_{C^{0,\alpha}(\bar{\Omega})}\big)$, and $\omega(x)$ is the modulus of uniform continuity of $\tilde{r}$.

The unique existence and the regularity is rather easily obtained from the method of characteristic and the Lemmas we have proven. The stability part is rather long but is a successive application of triangle inequalities.

proof of Theorem 2. Let $\mathbf{x} : \bar{E} \to \bar{\Omega}$ be the homeomorphism in Lemma 2.2.3. Then for any $\mathbf{x}_0 \in \bar{\Omega}$ there exist $0 \le s_0 \le L$ and $0 \le t_0 \le T$ such that $\mathbf{x}_0 = \mathbf{x}(s_0, t_0)$, i.e.,

$$\begin{aligned} &\frac{\partial}{\partial t}\mathbf{x}(s_0,t) = \mathbf{F}^{\perp}(\mathbf{x}(s_0,t)), \quad 0 \le t \le T, \\ &\mathbf{x}(s_0,0) \in \Gamma^{-}, \quad \mathbf{x}(s_0,t_0) = \mathbf{x}_0. \end{aligned}$$

If r is smooth, then we have following equivalence relations.

$$\begin{aligned} \nabla \times (r\mathbf{F}) = 0 &\iff (rf^2)_x - (rf^1)_y = -\mathbf{F}^{\perp} \cdot \nabla r + (f^2_x - f^1_y)r = 0 \\ &\iff -\frac{d}{dt} r(\mathbf{x}(s,t)) + (\nabla \times \mathbf{F})r = 0 \\ &\iff \frac{\frac{d}{dt} r(\mathbf{x}(s,t))}{r(\mathbf{x}(s,t))} = \nabla \times \mathbf{F}(\mathbf{x}(s,t)). \end{aligned} \tag{2.10}$$

Therefore, the resistivity r at $\mathbf{x}_0 = \mathbf{x}(s_0, t_0)$ should be given by

$$r(\mathbf{x}_0) = r(\mathbf{x}(s_0,0)) \exp\Big(\int_0^{t_0} \nabla \times \mathbf{F}(\mathbf{x}(s_0,\tau)) d\tau \Big). \tag{2.11}$$

Since the relations are equivalent this is the unique weak solution.

In the following, we will first show that $\big(r \circ \mathbf{x}\big)(s,t)$ has the regularity of $C^{0,\alpha}(\bar{E})$. Then the lemma 2.2.3 will imply $r(x,y) \in C^{0,\alpha}_{loc}(\Omega') \cap C^0(\bar{\Omega})$ as in statement of theorem 2 because $\mathbf{x}^{-1}(x,y)$ is only continuous in $\bar{\Omega}$ and differentiable merely in Ω'.

Let $\mathbf{x}_i \in \bar{\Omega}$ and $\mathbf{x}(s_i,t_i) = \mathbf{x}_i$ for $i = 1, 2$. First $\big(r \circ \mathbf{x}\big)(s,t)$ is differentiable with respect to t variable by (2.10). Also, $\mathbf{x}(s,t)$ is Lipschitz and $r_0(s)$ is hölder continuous on the boundary Γ^- with respect to s variable, hence their composition map $s \to r(\mathbf{x}(s,0))$ is also hölder continuous with respect to s variable. Similarly, the map $s \to e^{\left(\int_0^{t_0} \nabla \times \mathbf{F}(\mathbf{x}(s,\tau)) d\tau \right)}$ is hölder continuous and hence r in (2.11) is hölder continuous with respect to s variable because it is given by the product of those two maps. Therefore $r \circ \mathbf{x} \in C^{0,\alpha}(\bar{E})$ and hence $r = r \circ \mathbf{x} \circ \mathbf{x}^{-1} \in C^{0,\alpha}_{loc}(\Omega') \cap C^0(\bar{\Omega})$.

Now we show the stability, the second part of Theorem 2. Let $\tilde{\mathbf{F}}$ be another admissible vector field and $\tilde{\mathbf{x}} : \tilde{E} \to \Omega$ and $\tilde{r} : \bar{\Omega} \to \mathbb{R}$ be the corresponding diffeomorphism and resistivity, respectively. We assume $\Gamma^- = \tilde{\Gamma}^-$ and $\mathbf{x}(s,0) = \tilde{\mathbf{x}}(s,0)$ for $s \in [0, L]$ for here, which means the boundary measurements are same. We will show (2.9), for a fixed compact subset $K \subset \Omega'$. Let $\mathbf{x}_0 \in K$ be fixed and $\mathbf{x}_0 = \mathbf{x}(s_0,t_0) = \tilde{\mathbf{x}}(\tilde{s}_0, \tilde{t}_0)$ where $\Delta t := \tilde{t}_0 - t_0 \ge 0$ (see Figure 2.3 for an illustration). Consider, for $t \in [0, t_0]$,

$$\begin{aligned} &|\partial_t \mathbf{x}(s_0, t_0 - t) - \partial_t \tilde{\mathbf{x}}(\tilde{s}_0, \tilde{t}_0 - t)| \\ &\quad = |-\mathbf{F}^{\perp}(\mathbf{x}(s_0, t_0 - t)) + \tilde{\mathbf{F}}^{\perp}(\tilde{\mathbf{x}}(\tilde{s}_0, \tilde{t}_0 - t))| \\ &\quad \le |-\mathbf{F}^{\perp}(\mathbf{x}(s_0, t_0 - t)) + \tilde{\mathbf{F}}^{\perp}(\mathbf{x}(s_0, t_0 - t))| \\ &\quad + |-\tilde{\mathbf{F}}^{\perp}(\mathbf{x}(s_0, t_0 - t)) + \tilde{\mathbf{F}}^{\perp}(\tilde{\mathbf{x}}(\tilde{s}_0, \tilde{t}_0 - t))| \\ &\quad \le \|\mathbf{F} - \tilde{\mathbf{F}}\|_{\infty} + \|D\tilde{\mathbf{F}}\|_{\infty} |\mathbf{x}(s_0, t_0 - t) - \tilde{\mathbf{x}}(\tilde{s}_0, \tilde{t}_0 - t)|. \end{aligned}$$

Therefore, Gronwall's inequality gives, for $0 < t < t_0$,

$$|\mathbf{x}(s_0, t_0 - t) - \tilde{\mathbf{x}}(\tilde{s}_0, \tilde{t}_0 - t)| \le C \|\mathbf{F} - \tilde{\mathbf{F}}\|_{\infty}, \tag{2.12}$$

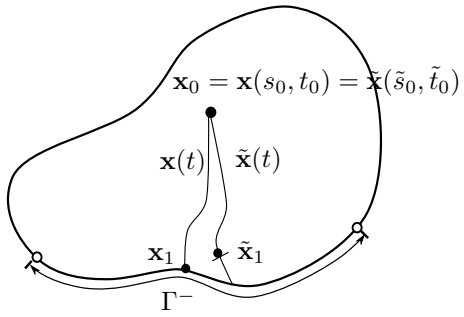

Figure 2.3: This figure is used as an illustration in the stability proof.

where $C = t_0 e^{t_0 \|D\tilde{F}\|_\infty}$.

Denote $\mathbf{x}_1 := \mathbf{x}(s_0, 0) \in \Gamma^-$, $\tilde{\mathbf{x}}_1 := \tilde{\mathbf{x}}(\tilde{s}_0, \Delta t) \in \Omega$, $h(t) := \nabla \times \mathbf{F}(\mathbf{x}(s_0, t))$ and $\tilde{h}(t) := \nabla \times \tilde{\mathbf{F}}(\tilde{\mathbf{x}}(\tilde{s}_0, t + \Delta t))$. Then, from (2.11),

$$r(\mathbf{x}_0) = r(\mathbf{x}_1) e^{\int_0^{t_0} h(t)\ dt}, \quad \tilde{r}(\mathbf{x}_0) = \tilde{r}(\tilde{\mathbf{x}}_1) e^{\int_0^{t_0} \tilde{h}(t+\Delta t) dt}.$$

Hence,

$$\begin{aligned}
&|r(\mathbf{x}_0) - \tilde{r}(\mathbf{x}_0)| \\
&\le \left| r(\mathbf{x}_1) e^{\int_0^{t_0} h(t)\ dt} - r(\mathbf{x}_1) e^{\int_0^{t_0} \tilde{h}(t)\ dt} \right| + \left| r(\mathbf{x}_1) e^{\int_0^{t_0} \tilde{h}(t)\ dt} - \tilde{r}(\tilde{\mathbf{x}}_1) e^{\int_0^{t_0} \tilde{h}(t)\ dt} \right| \\
&\le \|r_0\|_{C^0(\Gamma^-)} \left| e^{\int_0^{t_0} h(t)\ dt} - e^{\int_0^{t_0} \tilde{h}(t)\ dt} \right| + |r(\mathbf{x}_1) - \tilde{r}(\tilde{\mathbf{x}}_1)| \left| e^{\int_0^{t_0} \tilde{h}(t)\ dt} \right| \\
&\le \|r_0\|_{C^0(\Gamma^-)} \ \max\left(e^{\int_0^{t_0} h(t)\ dt}\ ,\ e^{\int_0^{t_0} \tilde{h}(t)\ dt} \right) \left| \int_0^{t_0} h(t) - \tilde{h}(t)\ dt \right| \\
&\qquad\qquad + |r(\mathbf{x}_1) - \tilde{r}(\tilde{\mathbf{x}}_1)| \left| e^{\int_0^{t_0} \tilde{h}(t)\ dt} \right| \\
&\le C\Big(\|h - \tilde{h}\|_\infty + |r(\mathbf{x}_1) - \tilde{r}(\tilde{\mathbf{x}}_1)| \Big),
\end{aligned}$$

where C depends on the quantities that the coefficient in (2.9) does. Now we estimate the two terms separately.

First, we have

$$\begin{aligned}
|r(\mathbf{x}_1) - \tilde{r}(\tilde{\mathbf{x}}_1)| &\le |r(\mathbf{x}_1) - \tilde{r}(\mathbf{x}_1)| + |\tilde{r}(\mathbf{x}_1) - \tilde{r}(\tilde{\mathbf{x}}_1)|. \\
&\le \|r_0 - \tilde{r}_0\|_\infty + \omega\big(|\mathbf{x}(s_0, 0) - \tilde{\mathbf{x}}(\tilde{s}_0, \Delta t)| \big) \\
&\le \|r_0 - \tilde{r}_0\|_\infty + \omega\big((C_1 \|\mathbf{F} - \tilde{\mathbf{F}}\|_\infty) \big),
\end{aligned}$$

where, in the second inequality, $\omega(x)$ is a modulus of uniform continuity of $\tilde{r}$. Also we used the fact that $\mathbf{x}_1 = \mathbf{x}(s_0, 0) = \tilde{\mathbf{x}}(s_0, 0) \in \Gamma^-$. Eq. (2.12) is used in the last inequality.

The other term is estimated by

$$\begin{aligned}
|h(t) - \tilde{h}(t)| &\le |\nabla \times \mathbf{F}(\mathbf{x}(s_0, t)) - \nabla \times \tilde{\mathbf{F}}(\tilde{\mathbf{x}}(\tilde{s}_0, t + \Delta t))| \\
&\le |\nabla \times \mathbf{F}(\mathbf{x}(s_0, t)) - \nabla \times \tilde{\mathbf{F}}(\mathbf{x}(s_0, t))| \\
&\quad + |\nabla \times \tilde{\mathbf{F}}(\mathbf{x}(s_0, t)) - \nabla \times \tilde{\mathbf{F}}(\tilde{\mathbf{x}}(\tilde{s}_0, t + \Delta t))| \\
&\le \|\mathbf{F} - \tilde{\mathbf{F}}\|_{C^1(\bar{\Omega})} + [D\tilde{\mathbf{F}}]_{C^{0,\alpha}(\bar{\Omega})} |\mathbf{x}(s_0, t) - \tilde{\mathbf{x}}(\tilde{s}_0, t + \Delta t)|^\alpha \\
&\le \|\mathbf{F} - \tilde{\mathbf{F}}\|_{C^1(\bar{\Omega})} + [D\tilde{\mathbf{F}}]_{C^{0,\alpha}(\bar{\Omega})} (C_1 \|\mathbf{F} - \tilde{\mathbf{F}}\|_\infty)^\alpha,
\end{aligned}$$

where estimate (2.12) is used again. Therefore we have

$$\begin{aligned}
&|r(\mathbf{x}_0) - \tilde{r}(\tilde{\mathbf{x}}_0)| \\
&\leq C_4\Big((C_1^\alpha[D\tilde{\mathbf{F}}]_{C^{0,\alpha}(\bar{\Omega})} + 1) + (C_1^\alpha[\tilde{r}]_{C^{0,\alpha}(K')} + 1)\Big) \\
&\Big(\|r_0 - \tilde{r}_0\|_\infty + \|\mathbf{F} - \tilde{\mathbf{F}}\|_\infty^\alpha + \|\mathbf{F} - \tilde{\mathbf{F}}\|_{C^1(\bar{\Omega})}\Big) \qquad (2.13) \\
&\leq C\Big(\|r_0 - \tilde{r}_0\|_\infty + \|\mathbf{F} - \tilde{\mathbf{F}}\|_{C^1(\bar{\Omega})}^\alpha\Big).
\end{aligned}$$

From calculations $C = C\big(\|F\|_{C^{1,\alpha}(\bar{\Omega})}, \|\tilde{F}\|_{C^{1,\alpha}(\bar{\Omega})}, \|r_0\|_{C^{0,\alpha}(\bar{\Omega})}, \|\tilde{r}_0\|_{C^{0,\alpha}(\bar{\Omega})}\big)$. Here we assumed $\|\mathbf{F} - \tilde{\mathbf{F}}\|_{C^1(\bar{\Omega})} < 1$ so that $\|\mathbf{F} - \tilde{\mathbf{F}}\|_{C^1(\bar{\Omega})} < \|\mathbf{F} - \tilde{\mathbf{F}}\|_{C^1(\bar{\Omega})}^\alpha$. □

Voltage construction

Now let us construct the voltage u from constructed r. It is well-defined up to an addition of a constant. If $r \in C^1(\Omega)$, then the existence of u that satisfies

$$-\nabla u = r\mathbf{F} \quad \text{in} \quad \bar{\Omega} \qquad (2.14)$$

is clear. Even if $r \in C^{0,\alpha}(\Omega)$ as in our case, the existence theory of such a $u \in H^1(\Omega)$ is classical (see Weyl [33]). Since $-\nabla u = r\mathbf{F}$ in Ω, we conclude $u \in C^{1,\alpha}_{loc}(\Omega') \cap C^1(\bar{\Omega})$.

We can also directly construct the u. Define $\tilde{u} : \bar{E} \to \mathbb{R}$ by

$$\begin{aligned}
\tilde{u}(s,0) &:= -\int_0^s r_0\big(\gamma(\tau)\big)\mathbf{F}\big(\gamma(\tau)\big) \cdot \gamma'(\tau) d\tau, \\
\tilde{u}(s,t) &:= \tilde{u}(s,0),
\end{aligned}$$

and $u : \bar{\Omega} \to \mathbb{R}$ by $u = \tilde{u} \circ \mathbf{x}^{-1}$. Then, one can easily see that $-r\mathbf{F} = \nabla u$ in $\bar{\Omega}$.

The optimal regularity of r

We obtained in Theorem 2 that $r \in C^{0,\alpha}_{loc}(\Omega') \cap C^0(\bar{\Omega})$. Also is true for σ if r is away from 0. If $r_0 > 0$, since the exponential term in (2.11) does not alter the sign, hence $r > 0$ in $\bar{\Omega}$. r has minimum in the compact domain thus is away from 0. Thus we will freely use r or σ for discussions.

We will show that the regularity cannot be improved. For a forward elliptic problem, $\sigma \in C^{1,\alpha}(\bar{\Omega})$ guarantees $\mathbf{J} \in C^{1,\alpha}(\bar{\Omega})$ and $\sigma \in C^{1,\alpha}(\Omega)$ guarantees $\mathbf{J} \in C^{1,\alpha}(\Omega)$ without boundary estimate. Our theorem says that the above sufficient conditions are not necessary conditions. We lose one derivative interior and even hölder continuity on boundary because sometimes less regular conductivity gives a regular $\mathbf{J}$. We have following examples.

First, we will show that we lose hölder continuity of σ on boundary, i.e., $r \notin C^{0,\alpha}(\bar{\Omega})$ in general. Consider an example,

$$r(x,y) := f(y) > 0, \quad u(x,y) := -\int_0^y f(y')\, dy'.$$

This is an example of one dimensional electrical current in two space dimensions and one can easily check that the electrical current is

$$\mathbf{J} = -\sigma\nabla u = \begin{pmatrix} 0 \\ 1 \end{pmatrix},$$

which is analytically smooth. Consider a domain given as in Figure 2.4(a), where a part of its boundary is along the line $y = -1$. According to Definition 2.2.1, this part of boundary belongs to Γ^0. Set $f(y) = 1 + |y+1|^{\frac{\alpha}{2}}$. This certainly does not belongs to $C^{0,\alpha}(\bar{\Omega})$ but belongs merely to $C^{0,\alpha}_{loc}(\Omega')$. Note

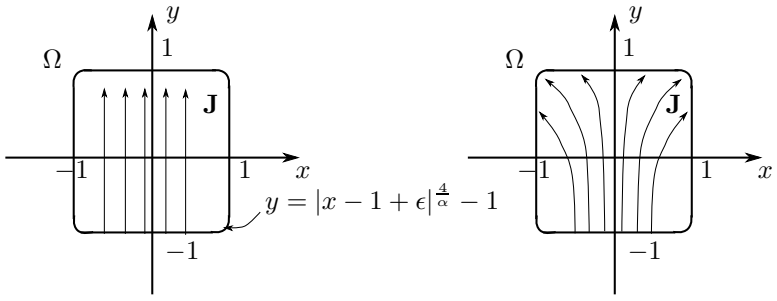

(a) domain of first example

(b) domain of second example

Figure 2.4: These illustrations are used to show the optimality in regularity theory.

that $r_0 \in C^{0,\alpha}(\Gamma^-)$, provided the curve at the corner of boundary is set as in Figure 2.4(a). One might even consider a discontinuous f, but this case is excluded by an assumption of Theorem 2 that $r_0 \in C^{0,\alpha}(\Gamma^-)$. We are considering a classical Schauder theory. In the case $r \notin C^{0,\alpha}_{loc}(\Omega')$.

In the next example we will see we lose one derivative inside of Ω, i.e., $r \notin C^{0,\beta}_{loc}(\Omega)$ for any $\beta > \alpha$. Let the domain be given as in Figure 2.4 (b) and let

$$r(x,y) := \frac{1}{\Big(1+|x|^{\frac{1}{2}}(1+y)\Big)^3} > 0, \quad u(x,y) := \frac{-x}{\Big(1+|x|^{\frac{1}{2}}(1+y)\Big)^2}.$$

Then, the electrical current is

$$\mathbf{J} = -\sigma\nabla u = \begin{pmatrix} 1 \\ -2x|x|^{\frac{1}{2}} \end{pmatrix},$$

which is $C^{1,\alpha}(\bar{\Omega})$. However $r \in C^{0,\alpha}(\Omega')$ but $r \notin C^{0,\beta}(\Omega')$ for any $\beta > \alpha$.

One might wonder an assumption in theorem 2 that r_0 to $C^{0,\alpha}(\bar{\Gamma^-})$ is a source of lowering regularities. However

$$r(\mathbf{x}_0) = r(\mathbf{x}(s_0,0)) \exp\Big(\int_0^{t_0} \nabla \times \mathbf{F}(\mathbf{x}(s_0,\tau))d\tau\Big),$$

and the regularity of r depends also on the the vector field $\mathbf{F}$, hence increasing the boundary regularity of r_0 to $C^{k,\alpha}(\bar{\Gamma^-})$ for $k \geq 1$ does not improve the regularity.

In summary, we optimally answered to the inverse Schauder solvability for $\sigma(x)$ and its by-product u.

2.3 Well-posedness of Orthotropic Resistivity Construction Problem

In this section, we assume that the resistivity is diagonal matrix field in a single coordinate system, i.e. $r = \begin{pmatrix} r^1 & 0 \\ 0 & r^2 \end{pmatrix}$. We try to solve a system of two partial differential equations

$$\begin{aligned} \nabla \times \big(r\mathbf{F_i}\big) = 0, \quad i = 1, 2, \quad \text{in } \Omega, \\ r^1 = r_0^1, \quad \text{on } \Gamma^1 \subset \partial\Omega, \\ r^2 = r_0^2, \quad \text{on } \Gamma^2 \subset \partial\Omega, \end{aligned} \tag{2.15}$$

with respect to the coefficients $\mathbf{F}_i = (F_i^x, F_i^y)$ and an initial conditions r_0^i defined on a portion Γ^i of the boundary for $i = 1, 2$.

From expansion of (2.15), we have

$$F_i^y\big(\partial_x r^2\big) - F_i^x\big(\partial_y r^1\big) + \big(\partial_x F_i^y\big)r^2 - \big(\partial_y F_i^1\big)r^1 = 0, \quad i = 1, 2.$$

Or

$$\begin{pmatrix} \partial_y r^1 \\ \partial_x r^2 \end{pmatrix} = \begin{pmatrix} -F_1^x & F_1^y \\ -F_2^x & F_2^y \end{pmatrix}^{-1} \begin{pmatrix} \partial_y F_1^x & -\partial_x F_1^y \\ \partial_y F_2^x & -\partial_x F_2^y \end{pmatrix} \begin{pmatrix} r^1 \\ r^2 \end{pmatrix} =: \mathbf{A}\Big(\mathbf{F}_i, \nabla\mathbf{F}_i\Big) \begin{pmatrix} r^1 \\ r^2 \end{pmatrix}, \tag{2.16}$$

provided that the matrix $\begin{pmatrix} -F_1^x & F_1^y \\ -F_2^x & F_2^y \end{pmatrix}$ is invertible. Thus we need the determinant $\mathbf{F}_1 \times \mathbf{F}_2 \neq 0$, i.e. the two vector fields are not parallel in any of the domain.

These are two waves propagate along x-axis and y-axis respectively. If wants, by introducing $t = \frac{x+y}{2}$ and $s = \frac{x-y}{2}$, the system can be written in the conventional form,

$$\begin{pmatrix} \big(\partial_t - \partial_s\big)r^1 \\ \big(\partial_t + \partial_s\big)r^2 \end{pmatrix} = \mathbf{A}\Big(\mathbf{F}_i, \nabla\mathbf{F}_i\Big) \begin{pmatrix} r^1 \\ r^2 \end{pmatrix}.$$

2.3.1 Admissibility of Data

The invertibility of $\begin{pmatrix} -F_1^x & F_1^y \\ -F_2^x & F_2^y \end{pmatrix}$ naturally induces the definition of admissibility for orthotropic conductivity construction problem.

Definition 2.3.1 (Admissibility 2)**.** *Let $\Omega \subset \mathbb{R}^2$ be a simply connected bounded open domain. Two smooth vector fields $\mathbf{F}_i$, i=1,2 are admissible in this section if $\mathbf{F}_1 \times \mathbf{F}_2 \neq 0$ in $\bar{\Omega}$.*

The following theorem can be found in literature for example in [17]. Here, we present a simpler proof for a completeness.

Theorem 3. *Suppose the conductivity σ, a symmetric positive definite matrix field is given in $\bar{\Omega}$. Then there is a choice of Neumann boundary conditions g^i, $i = 1, 2$, such that $\mathbf{J}^i = -\sigma\nabla u^i$ are admissible, where u^i is a solution of an elliptic equation*

$$\begin{aligned} \nabla \cdot (\sigma\nabla u^i) = 0, \quad \text{in } \Omega, \\ -\sigma\nabla u^i \cdot \mathbf{n} = g^i, \quad \text{on } \partial\Omega. \end{aligned}$$

proof of theorem 3. We may show the existence of two Dirichilet condition G^i, $i = 1, 2$ for ψ^i with the associated elliptic equation (2.2) so that $\mathbf{J}^i$ are admissible.

Let the total arc length of the boundary $L = 2\pi$ without loss. Let $G^1(\ell) = -\cos\ell$ and $G^2(\ell) = \sin\ell$. Then for both of G^1 and G^2, there is only one local maximum along the boundary. Since the boundary is assumed to be sufficiently smooth, one can extend G^i, $i = 1, 2$ into the $\bar{\Omega}$ smoothly. It is clear that only the local maxima along the boundary can be local maxima of extended functions along the boundary. By Alessandrini 2.1.1, $\nabla\psi^1$ and $\nabla\psi^2$ are non-vanishing in Ω. By Hopf's lemma, $\nabla\psi^i \neq 0$ along the boundary. We claim that $\nabla\psi^1 \times \nabla\psi^2$ also is non-vanishing in $\bar{\Omega}$. Suppose not. Then there is a point $\mathbf{x_0}$ such that $\nabla\psi^1(\mathbf{x_0}) = c\nabla\psi^2(\mathbf{x_0})$ for some constant c, which is finite since $\psi^i \in C^1$. Now consider $\tilde{\psi} = \psi^1 - c\psi^2$ which would have $\mathbf{x}_0$ as its critical point. By linearity, $\tilde{\psi}$ is a solution with boundary condition $\tilde{\psi}|_{\partial\Omega} = -\cos\ell - c\sin\ell = -\sqrt{(1+c^2)}\sin(\ell + \ell_*)$ for some ℓ_*. Since this boundary condition also has only one maximum, $\tilde{\psi}$ also cannot have a critical point, which contradicts our assumption. Since $\mathbf{J}_1 \times \mathbf{J}_2 = \nabla\psi^1 \times \nabla\psi^2$, proof is done. □

2.3.2 Main theorem

Our theorem goes with an assumption of convexity of domain for simplicity.

Lemma 2.3.1. *Let $\Omega \subset \mathbb{R}^2$ be a simply connected bounded and convex open set with smooth boundary. Then $\partial\Omega$ is a disjoint union of connected curves,*

$$\begin{aligned}\partial\Omega &= A_1^0 \cup \Gamma_1^- \cup B_1^0 \cup \Gamma_1^+, \\ &= A_2^0 \cup \Gamma_2^- \cup B_2^0 \cup \Gamma_2^+,\end{aligned}$$

such that

$$\begin{aligned}&(0,1)\cdot\mathbf{n} < 0, \quad \text{in } \Gamma_1^-, \quad (0,1)\cdot\mathbf{n} > 0, \quad \text{in } \Gamma_1^+, \quad (0,1)\cdot\mathbf{n} = 0, \quad \text{in } A_1^0 \text{ and } B_1^0, \\ &(1,0)\cdot\mathbf{n} < 0, \quad \text{in } \Gamma_2^-, \quad (1,0)\cdot\mathbf{n} > 0, \quad \text{in } \Gamma_2^+, \quad (1,0)\cdot\mathbf{n} = 0, \quad \text{in } A_2^0 \text{ and } B_2^0.\end{aligned}$$

In particular, A_i^0 is followed by Γ_i^- and B_i^0 is preceded by Γ_i^- in the counter-clockwise direction.

Proof. Let Arg be an angle function of a given vector. We take a branch so that $\text{Arg} : \mathbb{R}^2 \mapsto [0, 2\pi)$. Since $(0,1)\cdot\mathbf{n} = \cos\theta$, where $\theta = \text{Arg}\,(\mathbf{n}(\gamma(\ell)) - \pi/2$, the angle between two vectors $(0,1)$ and $\mathbf{n}$, we have $(0,1)\cdot\mathbf{n} = \sin\text{Arg}\,(\mathbf{n}(\ell))$. Now we define

$$\begin{aligned}\Gamma_1^+ &:= \{\gamma(\ell) \in \partial\Omega \mid \text{Arg}\,(\mathbf{n}(\ell)) \in (0, \ \pi)\}, \\ \Gamma_1^- &:= \{\gamma(\ell) \in \partial\Omega \mid \text{Arg}\,(\mathbf{n}(\ell)) \in (\pi, 2\pi)\}, \\ A_1^0 &:= \{\gamma(\ell) \in \partial\Omega \mid \text{Arg}\,(\mathbf{n}(\ell)) = 0)\}, \\ B_1^0 &:= \{\gamma(\ell) \in \partial\Omega \mid \text{Arg}\,(\mathbf{n}(\ell)) = \pi\},\end{aligned}$$

Since Arg is non-decreasing in convex domain, they are connected sets. Similarly, $(1,0)\cdot\mathbf{n} = \cos\theta$, where $\theta = \text{Arg}\,(\mathbf{n}(\gamma(\ell))$. We may define

$$\begin{aligned}\Gamma_2^+ &:= \{\gamma(\ell) \in \partial\Omega \mid \text{Arg}\,(\mathbf{n}(\ell)) \in [0, \pi/2) \cup (3\pi/2, 2\pi)\}, \\ \Gamma_2^- &:= \{\gamma(\ell) \in \partial\Omega \mid \text{Arg}\,(\mathbf{n}(\ell)) \in (\pi/2, 3\pi/2)\}, \\ A_2^0 &:= \{\gamma(\ell) \in \partial\Omega \mid \text{Arg}\,(\mathbf{n}(\ell)) = \ \pi/2\}, \\ B_2^0 &:= \{\gamma(\ell) \in \partial\Omega \mid \text{Arg}\,(\mathbf{n}(\ell)) = 3\pi/2\},\end{aligned}$$

In particular, A_i^0 is followed by Γ_i^- and B_i^0 is preceded by Γ_i^- in the counter-clockwise direction. □

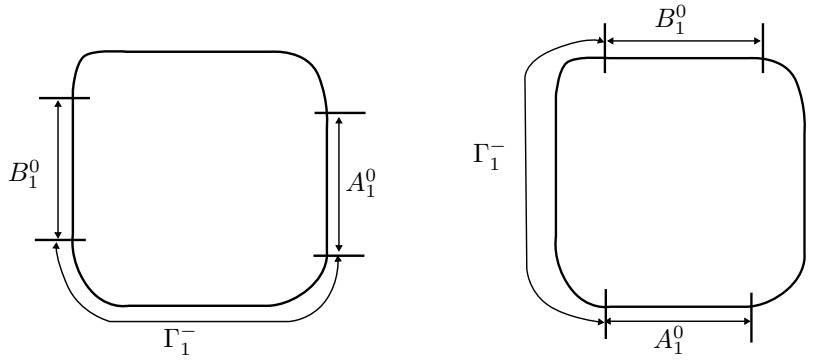

(a) Γ_1^-, A_1^0, and B_1^0 (b) Γ_2^-, A_2^0, and B_2^0

Figure 2.5: The geometry of boundary.

Theorem 4. *Let $\Omega \subset \mathbb{R}^2$ be a simply connected bounded open set with smooth boundary. Assume further that Ω is convex. Let $\Gamma_1^- := \{\mathbf{x} \in \partial\Omega \,|\, (0,1)\cdot\mathbf{n}(\mathbf{x}) < 0\}$, $\Gamma_2^- := \{\mathbf{x} \in \partial\Omega \,|\, (1,0)\cdot\mathbf{n}(\mathbf{x}) < 0\}$. Suppose that two admissible vector fields $\mathbf{F}_i$, $i = 1,2$ and smooth functions r_0^i on Γ_i^-, $i = 1,2$ are given. Then there exists unique diagonal matrix field $r = \begin{pmatrix} r^1 & 0 \\ 0 & r^2 \end{pmatrix}$ satisfying (2.15) such that*

$$r^1 \in C(\bar{\Omega}) \cap C^1\big(\bar{\Omega} \setminus A_1^0 \cup B_1^0\big) \quad r^2 \in C(\bar{\Omega}) \cap C^1\big(\bar{\Omega} \setminus A_2^0 \cup B_2^0\big).$$

Furthermore, if $\tilde{r}$ is the solution for admissible vector fields $\tilde{\mathbf{F}}_i$ with $\tilde{\Gamma}^- = \Gamma^-$ and a $\tilde{r}_0^i$, then

$$\|r - \tilde{r}\|_{L^\infty(\bar{\Omega})} \le C \sum_{i=1}^{2} \left(\|r_0^i - \tilde{r}_0^i\|_{L^\infty(\Gamma_i^-)} + \|\mathbf{F}_i - \tilde{\mathbf{F}}_i\|_{C^1(\bar{\Omega})} \right), \tag{2.17}$$

where $C = C\big(\|F\|_{C^{1,\alpha}(\bar{\Omega})}, \|\tilde{F}\|_{C^{1,\alpha}(\bar{\Omega})}, \|r_0\|_{C^{0,\alpha}(\bar{\Omega})}, \|\tilde{r}_0\|_{C^{0,\alpha}(\bar{\Omega})}\big)$.

Proof. Let $\Gamma_i^\pm$, A_i^0, and B_i^0 be the ones in Lemma 2.3.1, and let $\Gamma := \Gamma_1^- \cap \Gamma_2^- = \{\gamma(\ell) \in \partial\Omega \,|\, \mathrm{Arg}\,(\mathbf{n}(\ell)) \in (\pi/2, \pi)\}$. This is non-empty since $\partial\Omega$ is smooth boundary. Since B_1^0 is preceded by Γ_1^-, $(x_p, y_p) \in B_1^0$ is the one end point of Γ. Also $(x_q, y_q) \in A_2^0$ is the other end point of Γ. Consider an open domain D enclosed by two lines $y = y_p$ and $x = x_q$ and boundary portion c in Γ. The boundary portion c is characteristic on both end points and is not characteristic on other points. In this domain, the solution of (2.15) exists uniquely, such that

$$r^1 \in C(\bar{D}) \cap C^1\big(\bar{D} \setminus (x_q, y_q)\big) \quad r^2 \in C(\bar{D}) \cap C^1\big(\bar{D} \setminus (x_p, y_p)\big).$$

Well-posedness in $\bar{D}$ to obtain a solution with above regularity is classical, which is a successive application of fixed point argument. The failure of differentiability at the end points is due to the the fact that the curve c is characteristic on the points. Solution in the rest of domain is obtained by solving *Goursat Problem* successively to have the unique solution as in the statement. This process is solved stably under the perturbation of r_0^i and coefficients. Since coefficients in (2.15) are functions of $\mathbf{F}_i$ and $\nabla\mathbf{F}_i$, we have the stability estimates. □

2.4 Partial Well-posedness of Anisotropic Resistivity Construction Problem

In this section, we pose a system of equations on potentials. $\nabla \times (r\mathbf{J}_i) = 0$, $i = 1, 2, 3$ do not produce a hyperbolic system of three equations. The entries of r are not anymore eigenvalues for a fully anisotropic case. One may consider equations on two eigenvalues and an angle of the first eigenvector, but the analysis goes with non-linearity with them.

We assume that the three vector fields are all divergence-free in this section so that we can define the stream functions ψ^i, $i = 1, 2, 3$ of them. Thus We denote the data by $\mathbf{J}_i$.

In $\bar{\Omega}$, three Ohm's Laws are

$$r \begin{pmatrix} \psi^i_y \\ -\psi^i_x \end{pmatrix} = - \begin{pmatrix} u^i_x \\ u^i_y \end{pmatrix}, \quad i = 1, 2, 3.$$

In a region that the first two current vectors are not parallel, where $\mathbf{J}^1 \times \mathbf{J}^2 = -\psi^1_y \psi^2_x + \psi^2_y \psi^1_x \neq 0$, we can remove the matrix r from equations,

$$\begin{aligned} r \begin{pmatrix} \psi^1_y & \psi^2_y \\ -\psi^1_x & -\psi^2_x \end{pmatrix} &= - \begin{pmatrix} u^1_x & u^2_x \\ u^1_y & u^2_y \end{pmatrix}, \quad \text{or} \\ r &= - \begin{pmatrix} u^1_x & u^2_x \\ u^1_y & u^2_y \end{pmatrix} \begin{pmatrix} -\psi^2_x & -\psi^2_y \\ \psi^1_x & \psi^1_y \end{pmatrix} \frac{1}{-\psi^1_y \psi^2_x + \psi^2_y \psi^1_x}. \end{aligned} \tag{2.18}$$

The third Ohm's Law is then

$$- \begin{pmatrix} u^1_x & u^2_x \\ u^1_y & u^2_y \end{pmatrix} \begin{pmatrix} -\psi^2_x & -\psi^2_y \\ \psi^1_x & \psi^1_y \end{pmatrix} \frac{1}{-\psi^1_y \psi^2_x + \psi^2_y \psi^1_x} \begin{pmatrix} \psi^3_y \\ -\psi^3_x \end{pmatrix} = - \begin{pmatrix} u^3_x \\ u^3_y \end{pmatrix}.$$

We substituted r with (2.18). We may take curl operator on the both side

$$\nabla \times \left[- \begin{pmatrix} u^1_x & u^2_x \\ u^1_y & u^2_y \end{pmatrix} \begin{pmatrix} -\psi^2_x & -\psi^2_y \\ \psi^1_x & \psi^1_y \end{pmatrix} \frac{1}{-\psi^1_y \psi^2_x + \psi^2_y \psi^1_x} \begin{pmatrix} \psi^3_y \\ -\psi^3_x \end{pmatrix} \right] = 0. \tag{2.19}$$

which will remove u^3 also. It reduces the system to a single equation on two unknowns u^1 and u^2. Now, since r was symmetric, in the expansion of (2.18), the two anti-diagonal entries should agree, which gives us one more necessary equation

$$u^1_x \psi^2_y - u^1_y \psi^2_x = u^2_x \psi^1_y - u^2_y \psi^1_x. \tag{2.20}$$

Hence we can close the system for two unknowns u^1 and u^2.

In the neighborhood of a point such that $\mathbf{J}^1 \times \mathbf{J}^2 = -\psi^1_y \psi^2_x + \psi^2_y \psi^1_x$ does not vanish, the two stream lines themselves define a coordinate system since $-\psi^1_y \psi^2_x + \psi^2_y \psi^1_x$ is a determinant of a Jacobian $\begin{pmatrix} -\psi^2_x & \psi^1_x \\ -\psi^2_y & \psi^1_x \end{pmatrix}$ of the map $(-\psi_2, \psi_1)$. Let $(\xi, \eta) = (-\psi_2, \psi_1)$. Then

$$\begin{pmatrix} \partial_\eta \psi_1 \\ -\partial_\xi \psi_1 \end{pmatrix} = \begin{pmatrix} \partial_\eta \eta \\ -\partial_\xi \eta \end{pmatrix} = \begin{pmatrix} 1 \\ 0 \end{pmatrix}, \quad \begin{pmatrix} \partial_\eta \psi_2 \\ -\partial_\xi \psi_2 \end{pmatrix} = \begin{pmatrix} \partial_\eta (-\xi) \\ -\partial_\xi (-\xi) \end{pmatrix} = \begin{pmatrix} 0 \\ 1 \end{pmatrix}.$$

A version of Ohm's Laws as in (2.4) gives us

$$R \begin{pmatrix} 1 & 0 \\ 0 & 1 \end{pmatrix} = - \begin{pmatrix} u^1_\xi & u^2_\xi \\ u^1_\eta & u^2_\eta \end{pmatrix}.$$

From the symmetry condition of R, $u^1_\eta = u^2_\xi$, and we define a scalar ϕ such that $u^1 = \phi_\xi$ and $u^2 = \phi_\eta$. The third Ohm's law is

$$-\begin{pmatrix} u^1_\xi & u^2_\xi \\ u^1_\eta & u^2_\eta \end{pmatrix}\begin{pmatrix} \psi^3_\eta \\ -\psi^3_\xi \end{pmatrix} = -\begin{pmatrix} u^3_\xi \\ u^3_\eta \end{pmatrix}$$

and if we take the curl operator $\nabla_{(\xi,\eta)}\times$ on the both sides, what we obtain is,

$$\psi_{\eta\eta}u^1_\xi - \psi_{\xi\eta}(u^1_\eta + u^2_\xi) + \psi_{\xi\xi}u^2_\eta = 0.$$

We omit the superscript 3 in the third data. Finally we obtain

$$\psi_{\eta\eta}\phi_{\xi\xi} - 2\psi_{\xi\eta}\phi_{\xi\eta} + \psi_{\xi\xi}\phi_{\eta\eta} = 0. \tag{2.21}$$

Remark 2.4.1. *$R = D^2\phi$ and* (2.21) *corresponds to* (2.2)*. A symmetric and positive definite matrix coefficient in the equation is*

$$\begin{pmatrix} 0 & -1 \\ 1 & 0 \end{pmatrix} R \begin{pmatrix} 0 & 1 \\ -1 & 0 \end{pmatrix} = \begin{pmatrix} 0 & -1 \\ 1 & 0 \end{pmatrix} D^2\phi \begin{pmatrix} 0 & 1 \\ -1 & 0 \end{pmatrix} =: S.$$

Also, the first order terms are canceled out in (2.21)*.*

2.4.1 Admissibility of Data

The type of the second order linear equation (2.21) is determined by the sign of $\psi^2_{\xi\eta} - \psi_{\xi\xi}\psi_{\eta\eta}$ for each point. Be careful that the second derivatives of ψ are the coefficients and ϕ is the unknown. On the other hand, if we regard (2.21) an equation for ψ with coefficients given by ϕ, it is an elliptic equation without lower order terms as observed in Remark 2.4.1. It can be shown that any such ψ has a non-positive scalar curvature,

$$\psi_{\xi\xi}\psi_{\eta\eta} - \psi^2_{\xi\eta} \le 0$$

by following Lemma. Thus the type of the equation (2.21) is fixed to be hyperbolic but possibly degenerates.

Lemma 2.4.1 (from Gilbarg and Trudinger)**.** *If ψ is a solution of an uniformly elliptic equation without lower order terms, i.e.*

$$a\psi_{xx} + 2b\psi_{xy} + c\psi_{yy} = 0,$$

where $\begin{pmatrix} a & b \\ b & c \end{pmatrix}(x,y)$ is a symmetric positive definite matrix field satisfying uniform ellipticity condition, then $\psi_{xx}\psi_{yy} - \psi^2_{xy} \le 0$ and the equality holds only if $\psi_{xx} = \psi_{yy} = \psi_{xy} = 0$.

Proof. From uniform ellipticity the uniform ellipticity constant $\mu_0 > 0$,

$$\begin{aligned}\mu_0(\psi^2_{xx} + \psi^2_{xy}) &\le \left\langle \begin{pmatrix} a & b \\ b & c \end{pmatrix}\begin{pmatrix} \psi_{xx} \\ \psi_{xy} \end{pmatrix}, \begin{pmatrix} \psi_{xx} \\ \psi_{xy} \end{pmatrix} \right\rangle = a\psi^2_{xx} + 2b\psi_{xx}\psi_{xy} + c\psi^2_{xy} \\ &= (-2b\psi_{xy} - c\psi_{yy})\psi_{xx} + 2b\psi_{xx}\psi_{xy} + c\psi^2_{xy} \\ &= -c(\psi_{xx}\psi_{yy} - \psi^2_{xy}).\end{aligned}$$

Similarly we obtain

$$\begin{aligned}\mu_0(\psi^2_{xx} + \psi^2_{xy}) &\le \left\langle \begin{pmatrix} a & b \\ b & c \end{pmatrix}\begin{pmatrix} \psi_{xy} \\ \psi_{yy} \end{pmatrix}, \begin{pmatrix} \psi_{xy} \\ \psi_{yy} \end{pmatrix} \right\rangle \\ &= -a(\psi_{xx}\psi_{yy} - \psi^2_{xy}),\end{aligned}$$

and hence

$$\psi_{xx}\psi_{yy} - \psi_{xy}^2 \leq -\frac{\mu_0}{a+c}(\psi_{xx}^2 + 2\psi_{xy}^2 + \psi_{yy}^2) \leq 0.$$

□

Remember that we also needed that $\mathbf{J}^1 \times \mathbf{J}^2 \neq 0$ to derive (2.21). These lead us to define an admissibility of the data as follows.

Definition 2.4.1 (Admissibility 3)**.** *Let the domain Ω be as above. The vector fields $\mathbf{J}^i$, $i = 1, 2, 3$ that are smooth and divergence-free, are admissible in this section if*

1. *The map $\varphi(x, y) = \Big(\xi(x, y), \eta(x, y)\Big) := \Big(- \psi^2(x, y), \psi^1(x, y)\Big)$, where ψ^1 and ψ^2 are the stream functions of first two vector fields $\mathbf{J}^1$ and $\mathbf{J}^2$, are a diffeomorphism between $\bar{\Omega}$ and its image.*
2. *The scalar curvature of the stream function ψ of $\mathbf{J}^3$ with respect to the (ξ, η) coordinate system,*

$$\det D^2_{(\xi,\eta)} = \psi_{\xi\xi}\psi_{\eta\eta} - \psi_{\xi\eta}^2 < 0$$

   for all $(\xi, \eta) \in \varphi(\bar{\Omega})$.
3. *Along the boundary, the inner product $\big(D^2\psi\, T, T\big)$, where T is a unit tangent vector, has 4 simple zeroes.*

Let us explain the relevance of the definition. The first part is slightly stronger than the condition $\mathbf{J}_1 \times \mathbf{J}_2 \neq 0$ in $\bar{\Omega}$, which are the Jacobian determinant of the diffeomorphism. The second part also is stronger than the one automatically obtained by Lemma 2.4.1. We omitted the equality to exclude the degeneracy of equation.

The third part is related to the topological property. First let us remark the following observation.

Remark 2.4.2. *One can let $g := \frac{1}{\sqrt{-\det D^2\psi}} D^2\psi$, which is symmetric and has one positive and one negative eigenvalues. Then $\sqrt{-\det g}\; g^{-1} = \big(D^2\psi\big)^{-1}$. In other words, the equation (2.21) for ϕ is of a Laplace-Beltrami, the box operator $\Box_g$ with respect to the Lorentzian metric g.*

A Lorentzian manifold that admits a cauchy surface is called the *Globally Hyperbolic Lorentzian* manifold. A cauchy surface is a the *space-like* hypersurface, where every *time-like* curve intersect. The data on a cauchy surface determine the past as well as future of the function. Turning to our problem, in order to solve (2.21), we should have a cauchy surface, a cauchy curve for our 2-dimensional case, and the curve has to lie on $\partial\Omega$, where we only know the measurements on ϕ. The third condition is a sufficient condition to guarantee both of them. In general, a two dimensional simply connected Lorentizan manifold is not Globally Hyperbolic, but is *stably causal*. See [34] for more general contents.

We were able to present a theorem stating that the first condition and the second condition restricted in the interior Ω are achievable. It is remained to be an open question whether we can fill the gap between the status of stably causal to globally hyperbolic by only controlling boundary conditions. Here we left it as an assumption.

Theorem 5. *Suppose the conductivity σ, a symmetric positive definite matrix field is given in $\bar{\Omega}$. Then there is a choice of Neumann boundary conditions g^i, $i = 1, 2, 3$, such that $\mathbf{J}^i = -\sigma\nabla u^i$ satisfy the first condition and the second condition restricted in the interior Ω in Definition 2.4.1. Here u^i is a solution of an elliptic equation*

$$\begin{aligned} \nabla \cdot (\sigma \nabla u^i) &= 0, \quad \text{in } \Omega, \\ -\sigma\nabla u^i \cdot \mathbf{n} &= g^i, \quad \text{on } \partial\Omega. \end{aligned}$$

In order to prove Theorem 5, we introduce the following Lemma.

Lemma 2.4.2 (Meisters and Olech, 1963 [35]). *$\Omega \subset \mathbb{R}^n$ bounded and the boundary is Lipschitz. Let $y \in C^1(\bar{\Omega}; \mathbb{R}^n)$, $\det Dy > 0$ for $\forall x \in \bar{\Omega}$, $y|_{\partial\Omega}$ is one-to-one. Then y is bijective on $\bar{\Omega}$.*

proof of theorem 5. We may show the existence of three Dirichilet condition G^i, $i = 1, 2, 3$ for ψ^i with the associated elliptic equation so that $\mathbf{J}^i$ are admissible.

Let $\gamma(\ell)$ be the embedding of $\partial\Omega$ as before and let $G_1(\ell)$ and $G_2(\ell)$ be as in the proof of Theorem 1 and hence the ψ_1 and ψ_2 be the ones obtained from them. Then the determinant of Jacobian is nowhere vanishing, so it satisfies the first assumption of the Lemma 2.4.2 after flipping a sign if needed.

It is clear that the map $(-\psi^2, \psi^1)|_{\partial\Omega}$ is injective since $\ell \in [0, 2\pi] \mapsto (-G^2(\ell), G^1(\ell)) = (\cos\ell, \sin\ell)$ is injective. From the Lemma of Meisters and Olech, the map $\varphi := (-\psi^2, \psi^1)$ is bijective in $\bar{\Omega}$. The differentiability of the map and its inverse come from the inverse function theorem. Therefore we proved the first assertion that we can generate $\mathbf{J}^1$ and $\mathbf{J}^2$ satisfying the first admissibility condition.

Now, we prove the rest. Now we have the diffeomorphism so we use the (ξ, η) coordinate system. One can see that $\varphi(\bar{\Omega})$ is a unit disk. As the discussion earlier, the third stream function ψ is a solution of (2.21), which is a uniformly elliptic equation without lower order terms. Here ψ is unknown and the second derivatives of ϕ are coefficients. By Lemma 2.4.1, we only need to prove $D^2\psi$ is not a zero matrix for all points in $\bar{\Omega}$ to prove the second assertion.

Now we claim that if the boundary condition $G^3(\ell)$ is set to be $\cos(2\ell)$, then there is no point in $\bar{\Omega}$ such that the Hessian becomes zero matrix.

Suppose there is a point (ξ_0, η_0) such that $D^2\psi(\xi_0, \eta_0) = 0$. Suppose $\nabla\psi(\xi_0, \eta_0) = (c_1, c_2)$. c_1 and c_2 are finite since ψ is C^1. Now consider $\tilde{\psi} := \psi - c_1\xi - c_2\eta$, then its Hessian is not changed, but now $\tilde{\psi}$ has (ξ_0, η_0) as its critical point, in particular of multiplicity 2, since its Hessian vanishes at the point. By linearity, $\tilde{\psi}$ is a solution with a boundary condition $\tilde{G}(\ell) = \cos(2\ell) - c_1\cos(\ell) - c_2\sin(\ell)$. In order to investigate the local maxima along the boundary, differentiate G with respect to ℓ to obtain

$$G'(\ell) = -2\sin(2\ell) + c_1\sin(\ell) - c_2\cos(\ell) = -4\cos(\ell)\sin(\ell) + c_1\sin(\ell) - c_2\cos(\ell).$$

Now consider an auxiliary function $\alpha(\xi, \eta) := -4\xi\eta + c_1\eta - c_2\xi$ that coincides with $G'(\ell)$ on the boundary. The zero set of α contains the zero set of $G'(\ell)$, which is the intersection point of the unit circle and the zero set of α. The zero set of α ins a hyperbola if $c_1^2 + c_2^2 \neq 0$, and is a two straight lines otherwise. Therefore the number of intersection points with the unit circle is at most 4 and hence the number of maxima is at most 2. By Alessandrini, $\tilde{\psi}$ cannot have a critical point of multiplicity 2, which contradicts our assumption. Therefore there is no interior point such that the Hessian becomes zero matrix. By lemma, we conclude that $\psi_{\xi\xi}\psi_{\eta\eta} - \psi_{\xi\eta}^2 < 0$ in Ω.

□

2.4.2 Main Theorem

We are going to prove our main theorem stated as follows.

Theorem 6. *Let $\Omega \subset \mathbb{R}^2$ be a simply connected bounded open set with smooth boundary. Suppose that admissible vector fields $\mathbf{J}_i$, $i = 1, 2, 3$ are given, and $\mathbf{N}_1$ and $\mathbf{N}_2$ be the two characteristic vector fields defined by Lemma 2.4.3. Let $\Gamma_1^- := \{\mathbf{x} \in \partial\Omega \,|\, \mathbf{N}_1 \cdot \mathbf{n}(\mathbf{x}) < 0\}$, and $\Gamma_2^- := \{\mathbf{x} \in \partial\Omega \,|\, \mathbf{N}_2 \cdot \mathbf{n}(\mathbf{x}) < 0\}$. Also*

the voltage information on u^1 and u^2 are given on Γ_i^-, $i = 1, 2$ by the following form.

$$(u^1, u^2) \cdot \mathbf{N}_2 = v_1^0, \quad \text{on } \Gamma_1^-,$$
$$(u^1, u^2) \cdot \mathbf{N}_1 = v_2^0, \quad \text{on } \Gamma_2^-.$$

Then, there exists a unique symmetric matrix field $r \in C(\Omega)$, and voltages u^1 and u^2 such that r is given by the formula (2.18)*, and u^1 and u^2 are the solution of* (2.19)-(2.20) *with above boundary conditions.*

In order to prove our main Theorem 6, we first prove several Lemmas.

Lemma 2.4.3 (Proposition 3.37 in [34])**.** *Let (M, g) be a simply connected Lorentzian manifold of dimension two. Then two smooth nonvanishing null vector fields X_1 and X_2 may be defined on M such that X_1 and X_2 are linearly independent at each point of M.*

In this thesis, we will denote $\mathbf{N}_1$ and $\mathbf{N}_2$ instead of X_1 and X_2.

Corollary 2.4.1. *We may define two smooth nonvanishing linearly independent vector fields $\mathbf{N}_1$ and $\mathbf{N}_2$ on $\bar{\Omega}$ that are characteristic everywhere for the equation* (2.21) *if $\mathbf{J}_i$ are admissible data.*

Proof. Let φ be the diffeomorphism in the admissibility condition and $U = \varphi(\Omega)$. For a fixed point, the two characteristic vectors are given by the kernel of

$$Q : V \mapsto \langle D^2\psi \; V, V \rangle.$$

Existence of two such directions comes from the second condition of admissibility, the strict hyperbolicity of (2.21). $\mathbf{N}_1$ and $\mathbf{N}_2$ can be defined by Lemma 2.4.3 for a Lorentzian manifold $\left(\bar{U}, g = D^2_{\xi,\eta}\psi\right)$. Since characteristic directions are invariant under a diffeomorphism, the assertion is followed. □

Lemma 2.4.4. *Let $\Omega \subset \mathbb{R}^2$ be a simply connected bounded open set with smooth boundary. Let $\mathbf{J}_i$, $i = 1, 2, 3$ admissible data. Let $\mathbf{N}_1$ and $\mathbf{N}_2$ be the two characteristic vector fields. Then $\partial\Omega$ is a disjoint union of connected curves,*

$$\begin{aligned} \partial\Omega &= A_1^0 \cup \Gamma_1^- \cup B_1^0 \cup \Gamma_1^+, \\ &= A_2^0 \cup \Gamma_2^- \cup B_2^0 \cup \Gamma_2^+, \end{aligned}$$

such that

$$\begin{aligned} &\mathbf{N}_1 \cdot \mathbf{n} < 0, \quad \text{in } \Gamma_1^-, \quad \mathbf{N}_1 \cdot \mathbf{n} > 0, \quad \text{in } \Gamma_1^+, \quad \mathbf{N}_1 \cdot \mathbf{n} = 0, \quad \text{in } A_1^0 \text{ and } B_1^0, \\ &\mathbf{N}_2 \cdot \mathbf{n} < 0, \quad \text{in } \Gamma_2^-, \quad \mathbf{N}_2 \cdot \mathbf{n} > 0, \quad \text{in } \Gamma_2^+, \quad \mathbf{N}_2 \cdot \mathbf{n} = 0, \quad \text{in } A_2^0 \text{ and } B_2^0. \end{aligned}$$

In particular, A_i^0 is followed by Γ_i^- and B_i^0 is preceded by Γ_i^- in the counter-clockwise direction.

Proof. Since $\mathbf{N}_1$ and $\mathbf{N}_2$ are nowhere vanishing vector fields, the winding number of each of them along the $\partial\Omega$ is zero. Therefore $\mathrm{Arg}\,(\mathbf{N}_i)$ is a periodic function within a one branch of Arg function. On the other hand, $\mathrm{Arg}\,(T)$ of a tangent vector along the boundary takes all angles in a one branch. Thus $\mathrm{Arg}\,(\mathbf{N}_1)$ and $\mathrm{Arg}\,(\mathbf{n})$ intersects at least once along the boundary by continuity. Similarly, $\mathrm{Arg}\,(-\mathbf{N}_1)$, $\mathrm{Arg}\,(\mathbf{N}_2)$, and $\mathrm{Arg}\,(-\mathbf{N}_1)$ also intersect $\mathrm{Arg}\,(T)$ at least once respectively. Since $\mathrm{Arg}\,(N_i)$ and $\mathrm{Arg}\,(-N_i)$ always have different values, and $\pm(\mathbf{N}_1 \times \mathbf{N}_2) \neq 0$, those intersection points are all disjoint. The third condition in the admissibility implies that there are only 4 connected components of boundary whose tangent vector is characteristic, i.e. the intersection points. Therefore 4 components correspond to each of intersection points.

Hence, we may define A_1^0 and B_1^0, whose tangent vectors have same Arg values with $\mathbf{N}_1$ and $-\mathbf{N}_1$ respectively. Then $\mathbf{N}_1 \cdot (n_1, n_2) = \mathbf{N}_1 \times (-n_2, n_1) = \mathbf{N}_1 \times T = 0$ on the two set. There are no other points in $\partial\Omega$ such that $\mathbf{N}_1 \times T = 0$. Now define Γ_1^- be the one of two curves joining A_1^0 and B_1^0 so that one $\mathbf{N}_1 \cdot \mathbf{n} < 0$, and Γ_1^+ be the other curve. Similarly we define, A_2^0, B_2^0 and $\Gamma_2^\pm$. We may flip the definition of A_i^0 and B_i^0 so that the appearing order along counter-clockwise direction is as in the statement. □

Lemma 2.4.5. *Let $\Omega \subset \mathbb{R}^2$ be a simply connected bounded open set with smooth boundary. Let $\mathbf{J}_i$, $i = 1, 2, 3$ be an admissible data, and $\mathbf{N}_1$ and $\mathbf{N}_2$ be the two characteristic vector fields. Then there are two functions $\nu_1(x, y)$ and $\nu_2(x, y)$ such that $\nu := (\nu_1, \nu_2)$ is a C^1-diffeomorphsm between $\bar{\Omega}$ and its image.*

Proof. Observe that $\mathbf{N}_1^\perp$ and Γ_1^- consist an admissible data for an isotropic problem of Definition 2.2.1. Therefore for an appropriate smooth initial data ρ_0, we can define C^1 potential function u as in (2.14) such that

$$\nabla \times (\rho \mathbf{N}_1^\perp) = 0, \quad -\rho \mathbf{N}_1^\perp = \nabla u, \quad \rho > 0.$$

Denote ν_1 be the potential u, then $\nabla\nu_1$ is nowhere vanishing and parallel to $\mathbf{N}_1^\perp$, i.e. the level curves of ν_1 are parallel to $\mathbf{N}_1$.

Similarly, define ν_2 with $\mathbf{N}_2$. The determinant of Jacobian is nowhere vanishing since $\mathbf{N}_1 \times \mathbf{N}_2 \neq 0$.

By Lemma (2.4.2), we only need to prove the map ν is injective on the boundary. Since ρ was positive, ν_1 and ν_2 are strictly monotone on Γ_1^- and Γ_2^- respectively. They are also strictly monotone on Γ_1^+ and Γ_2^+ by Lemma 2.2.2. Since on A_1^0 and B_1^0, where ν_1 is constant, are subsets of $\Gamma_2^- \cup \Gamma_2^+$, ν_2 is monotone. On the other hand, A_2^0 and B_2^0, where ν_2 is constant, are subsets of $\Gamma_1^- \cup \Gamma_1^+$, and thus ν_1 is monotone. Therefore $\nu|_{\partial\Omega}$ is injective.

□

Now we prove the main theorem.

proof of Theorem 6. Let $\nu := (\nu_1, \nu_2)$ be the C^1 diffeomorphism, and $W := \nu(\Omega)$. Since the level curves of ν_1 and ν_2 are characteristic lines, (2.21) can be written as

$$2\phi_{\nu_1\nu_2} - a\phi_{\nu_1} - b\phi_{\nu_2} = 0, \tag{2.22}$$

where a and b are two functions of $\psi_{\xi\xi}$, $\psi_{\xi\eta}$ and $\psi_{\eta\eta}$ at each point. Let $v_1 = \phi_{\nu_1}$ and $v_2 = \phi_{\nu_2}$. Then

$$\begin{aligned} \partial_{\nu_2} v_1 - \partial_{\nu_1} v_2 &= 0, \\ \partial_{\nu_2} v_1 + \partial_{\nu_1} v_2 &= a v_1 + b v_2, \end{aligned}$$

or

$$\begin{pmatrix} \partial_{\nu_2} v_1 \\ \partial_{\nu_1} v_2 \end{pmatrix} = \mathbf{A}(a, b) \begin{pmatrix} v_1 \\ v_2 \end{pmatrix}.$$

These equations on two unknowns v_1 and v_2 consists an exactly same structure of system (2.16). Together with v_1^0 on Γ_1^- and v_2^0 on Γ_2^-, by Theorem 4, we conclude that there exists unique solution v_1 and v_2 such that

$$v_1 \in C^1\big(\bar{W} \setminus A_1^0 \cup B_1^0\big), \quad v_2 \in C^1\big(\bar{W} \setminus A_2^0 \cup B_2^0\big).$$

Since ν was C^1 map, we may conclude that

$$v_1 \in C^1\big(\bar{\Omega} \setminus A_1^0 \cup B_1^0\big), \quad v_2 \in C^1\big(\bar{\Omega} \setminus A_2^0 \cup B_2^0\big).$$

Remember that $u^1 = \phi_\xi$ and $u^2 = \phi_\eta$. Note that in the interior Ω, u^1 and u^2 are C^1. From the formula (2.18), there exists a unique symmetric matrix field $r \in C(\Omega)$. □

Chapter 3. Numerical Algorithm to Construct Resistivity

In this chapter, we solve numerically the equation

$$\begin{aligned} \nabla \times (r\mathbf{F}) = 0, \quad &\text{in } \Omega, \\ r = r_0, \quad &\text{on } \Gamma \subset \partial\Omega. \end{aligned} \tag{3.1}$$

and the system

$$\begin{aligned} \nabla \times \left(\begin{pmatrix} r^1 & 0 \\ 0 & r^2 \end{pmatrix} \mathbf{F}_i \right) = 0, \quad i = 1, 2, \quad &\text{in } \Omega, \\ r^1 = r_0^1, \quad &\text{on } \Gamma^1 \subset \partial\Omega, \\ r^2 = r_0^2, \quad &\text{on } \Gamma^2 \subset \partial\Omega, \end{aligned} \tag{3.2}$$

respectively, where r, r^1, and r^2 are real-valued functions, and Γ, Γ^1 Γ^2 are portions of $\partial\Omega$.

Each of them are solved numerically by mimetic difference method. The mimetic method is a kind of difference method that in particular mimics class of covariant operators such as *gradient, curl, divergence, laplacian, and etc* with very high accuracy. Those who want more general information are referred to [36], [37], [38], [39] and [40]. In Strang [36], we can find things that we only need to apply the method in terms of circuit theory. There, the physics $\nabla \cdot \mathbf{J}$ and $\nabla \times \mathbf{E} = 0$ are mimicked by Kirchoff's Current and Voltage Laws.

Recall that the equation (3.1) and the system (3.2) were solved by applying tools for hyperbolic equations in the preceding chapter. It will be seen in detail how the hyperbolic nature and the physics are treated together in peace.n

3.1 Virtual Resistive Network : A mimetic discretization

In a mimetic discretization, values of various fields are assigned delicately. Consider mesh $(x^i, y^j) \in \boldsymbol{R}^2$ with $0 \le i, j \le n$ in Figure 3.1 Vector fields such as the current density $\mathbf{J}$ or the electrical field $\mathbf{E}$ is assigned along edges. (see Figure 3.1(b)) For example, $E^{i+\frac{1}{2}j}$ is the component of the electrical field $\mathbf{E}$ in the direction connecting two mesh points (x^i, y^j) and (x^{i+1}, y^j). Notice that $(x^{i+\frac{1}{2}}, y^j)$ denotes the midpoint of the this edge. (see Figure 3.1(b)). Notice no full vector are assigned on a same site. A discrete version of a $\nabla \times \mathbf{E}$ is approximated by

$$E^{i+\frac{1}{2}\,j} + E^{i+1\,j+\frac{1}{2}} - E^{i+\frac{1}{2}\,j+1} - E^{i-1\,j+\frac{1}{2}}.$$

for a cell enclosed by edges. The Kirchoff's Voltage Law is a statement that the the expression vanishes for all cells.

If E^{ij} satisfies the Kirchoff's Voltage Law, it admits a scalar potential u that is assigned at vertices. The potential values are assumed to approximate $u^{ij} \cong u(x^i, y^j)$ (see Figure 3.1(a)). Then, we may set

$$E^{i+\frac{1}{2}\,j} = -\frac{u^{i+1\,j} - u^{i\,j}}{x^{i+1} - x^i}, \qquad E^{i\,j+\frac{1}{2}} = -\frac{u^{i\,j+1} - u^{i\,j}}{y^{j+1} - y^j} \tag{3.3}$$

On the while, a discrete version of a $\nabla \cdot \mathbf{F}$ is approximated by

$$F^{i+\frac{1}{2}\,j} - F^{i+\frac{1}{2}\,j} + F^{i\,j+\frac{1}{2}} - F^{i\,j-\frac{1}{2}}.$$

at a vertex (i, j). The Kirchoff's Current Law is a statement that the expression vanishes for all vertices.

If $\mathbf{F}$ is an incompressible vector field, i.e., $\nabla \cdot \mathbf{F} = 0$, then it is convenient to consider a *stream function* ψ that satisfies

$$\mathbf{F} = \nabla^{\perp}\psi, \quad \text{where } \nabla^{\perp} := \begin{pmatrix} \partial_y \\ -\partial_x \end{pmatrix}.$$

The F^{ij} satisfying Kirchoff's Current Law admits a discrete version of a stream function. The value of the stream function is assigned to the midpoint of each cell, i.e., $\psi^{i+\frac{1}{2}\,j+\frac{1}{2}} \cong \psi(x^{i+\frac{1}{2}}, y^{j+\frac{1}{2}})$(see Figure 3.1(c)). Then, $\mathbf{F}$ is given by

$$F^{i+\frac{1}{2}j} = \frac{\psi^{i+\frac{1}{2}\,j+\frac{1}{2}} - \psi^{i+\frac{1}{2}\,j-\frac{1}{2}}}{y^{j+\frac{1}{2}} - y^{j-\frac{1}{2}}}, \qquad F^{ij+\frac{1}{2}} = -\frac{\psi^{i+\frac{1}{2}\,j+\frac{1}{2}} - \psi^{i-\frac{1}{2}\,j+\frac{1}{2}}}{x^{i+\frac{1}{2}} - x^{i-\frac{1}{2}}}. \tag{3.4}$$

If $\nabla \cdot \mathbf{F} \neq 0$, we will take the divergence free part of the Helmholtz decomposition of the field $\mathbf{F}$.

The conductivity and the resistivity are given by Ohm's Law, $\mathbf{J} = \sigma\mathbf{E}$ or $\mathbf{E} = r\mathbf{J}$. Therefore, it is natural to assign them along the edges. Hence, we set

$$\begin{array}{l} J^{i+\frac{1}{2}\,j} = \sigma^{i+\frac{1}{2}\,j}E^{i+\frac{1}{2}\,j}, \\ J^{i\,j+\frac{1}{2}} = \sigma^{i\,j+\frac{1}{2}}E^{i\,j+\frac{1}{2}}, \end{array} \quad \text{or} \quad \begin{array}{l} E^{i+\frac{1}{2}\,j} = r^{i+\frac{1}{2}\,j}J^{i+\frac{1}{2}\,j}, \\ E^{i\,j+\frac{1}{2}} = r^{i\,j+\frac{1}{2}}J^{i\,j+\frac{1}{2}}. \end{array} \tag{3.5}$$

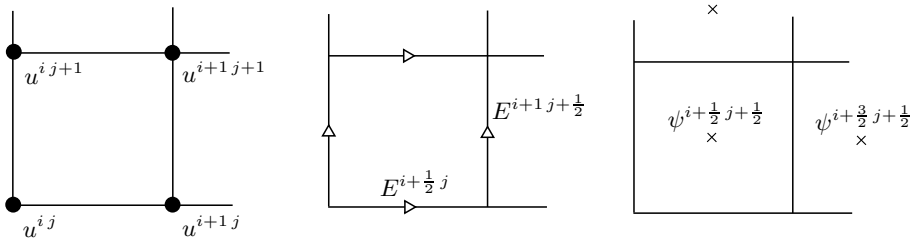

(a) potential function (b) vector field (c) stream function

Figure 3.1: Mimetic discretization: The potentials are assigned at vertices, the electrical fields are assigned along the edges, and stream functions are in cells.

This mimetic approach is identical to the resistive network system given in Figure 3.2. This resistive network has been virtually made from a continuous conductivity body as a discretization method and we will call it a *virtual resistive network* (or VRN for brevity). The use of these mimetic discretization reduces computation error. For example, the sum of edge values of $\mathbf{E}$ along any closed loop in the network automatically becomes zero, which is not the case of a finite difference method. In other words, Kirchoff's law of voltage is exactly satisfied and hence the main part of the computation error is from the data, but not from the discretization of the problem.

Remark 3.1.1. *The network system naturally approximates an orthotropic resistivity. If we make use of full degrees of freedom to assign r values in vertical and horizontal edges, then it reflects that the resistivity at a local point has different eigenvalues along the two directions. Since we have constructed only rectangular network, the eigenvectors are all fixed to be aligned to axes, which means the resistivity field is globally diagonalized orthotropic one.*

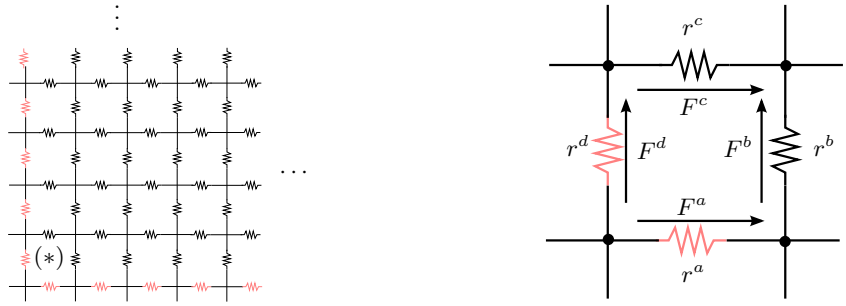

(a) VRN (b) components of a cell

Figure 3.2: A network. If the resistivity values of boundary resistors along two sides of the domain, the colored (or grey) ones, are given, the others can be computed by a cell by cell local computation.

3.2 Virtual Resistive Network for Isotropic Materials

In this section we develop a numerical algorithm which is based on a virtual resistive network system. For simplicity, we construct a square network in this section. However, the algorithm comes from a contour integration of an arbitrary network system and one may develop various shapes of network system depending on the geometry of a given problem. Since the network system plays as a background of the discretization, one may rotate it as in Figure 3.7 and obtain various reconstructed images to compare the noise effects using a single set of current data. This reconstruction algorithm has a nature of hyperbolic problems such as the noise propagation along characteristics and the domains of dependence and influence. In the simulation we investigate the effect of multiplicative and additive noises. The computation cost of the algorithm is very low since the conductivity is obtained from a cell by cell local computation. Hence we may save a concern of the convergence of an iterative algorithm and do three dimensional computations easily.

The numerical simulation results are compared with an equipotential line and a direct integration methods [16, 15, 11]. The VRN method developed in this section provides much better conductivity images than other methods. The key of the conductivity reconstruction is to reduce the noise propagation along characteristic lines which is the source of noisy stripes in the reconstructed images. The VRN method reduces the appearance of such stripes. However, if the noise level becomes as big as 30% as in Figure 3.15(c), such stripes appear again. One may develop various shapes of network system (see [13]) or apply two sets of current data with perpendicular characteristic lines to reduce the appearance of the noisy stripes.

3.2.1 Properties of Rectangular VRN : Isotropic

We derive a conductivity construction algorithm using a VRN (virtual resistive network) and investigate its property. The network gives basic structures of VRN and one may develop other shapes of VRN to improve its performance. For a presentational simplicity we consider a domain $\Omega = (0,1)\times(0,1)$ and the boundary $\Gamma = \{0\}\times[0,1]\cup[0,1]\times\{0\} \subset \partial\Omega$. However, one may handle any shape of domain by simply placing it on the VRN. In fact, the simulations in Section 3.2.3 are for a circular domain placed on the network developed in this section. The mesh points (x^i, y^j) are with $0 \le i, j \le n$. Hence there are $(n+1)^2$ vertices, $2n(n+1)$ edges, and n^2 cells. We assume that the boundary resistivity r_0 is given along the edges on the boundary Γ (see Figure 3.2(a)). In other words, $2n$ number of resistors are given

initially and therefore, our job is to decide the other $2n^2$ resistors.

Let D be the area of a cell (see Figure 3.2(b)). Then, the integration of (3.1) over the area D gives

$$0 = \int_D \nabla \times (r\mathbf{F})dx = \oint_{\partial D} r\mathbf{F}(z)dz.$$

We will assume that each edge has the same unit length. Then, the resistor and resistivity are equivalent. For convenience, we denote the resistor and the current density as in Figure 3.2(b). Then, the above equation is written as

$$r^a F^a + r^b F^b - r^c F^c - r^d F^d = 0, \tag{3.6}$$

which is also called Kirchoff's voltage law. Note that there are n^2 number of cells and hence n^2 equations. Therefore the number of equations are not enough to decide $2n^2$ unknown resistors. If two sets of current data are given, say $\mathbf{F}_1$ and $\mathbf{F}_2$, then we obtain $2n^2$ equations and those unknowns can be decided. In the case r^c gives a conductivity in horizontal direction and r^b in vertical direction. In other words, we may actually obtain orthotropic conductivity. For an *isotropic* case, we assume

$$r^b = r^c. \tag{3.7}$$

Then, the total number of unknowns are n^2. Suppose that two resistors r^a and r^d have been obtained in previous steps or initially. One can find such a cell from Figure 3.2(a), which is at the left bottom corner. Then, the above relation gives

$$r^b = \frac{r^d F^d - r^a F^a}{F^b - F^c} \quad \text{if} \quad F^b \neq F^c. \tag{3.8}$$

If r^b and r^c are decided, then we have another cell with two given resistors and hence we may continue and find all resistors. Notice that, if $F^b - F^c \cong 0$, we cannot obtain the resistivity. The admissibility condition is actually related to avoid such a situation (see Section 3.2.1).

Remark 3.2.1 (Anisotropic Resistivity)**.** *The assumption (3.7) restricts the orthotropic case to the isotropic case.*

Admissibility of Boundary

Recall that the resistivity could be constructed under the condition that the boundary Γ and the field $\mathbf{F}$ are admissible. Here, we consider the domain $\Omega = (0,1) \times (0,1)$ and the boundary $\Gamma = \{0\} \times [0,1] \cup [0,1] \times \{0\}$. This choice of boundary allows the existence of a cell with two given resistors (r^a and r^d in Figure 3.2(b)) all the time. If a different boundary is chosen, then the algorithm should be modified appropriately. Notice that, if $F^b - F^c \cong 0$ in Equation (3.8), we cannot obtain the resistivity. In the following discussion we fix the boundary Γ and consider the effect of the direction of currents.

In Figure 3.3 three examples of recovered conductivity are given with fixed same Γ for all cases. Three different current densities are considered, where the currents were injected through two electrodes on the boundary denoted with arrows in the figures. Since an admissible boundary Γ^- is where the vector fields orthogonal to $\mathbf{J}$ is in inward direction, the case of Figure 3.3(c) is the only case that the boundary we fixed is admissible. Note that the conductivity has been reconstructed completely only for this case. This example explains the importance of having an admissible boundary and current density.

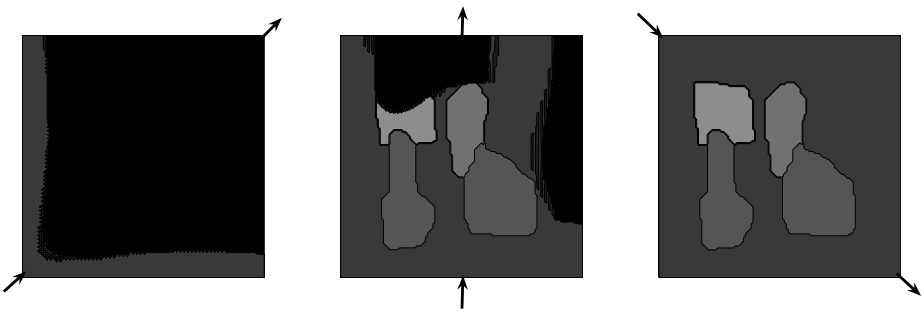

(a) nothing recovered (b) partly recovered (c) fully recovered

Figure 3.3: Two dimensional isotropic conductivity has been recovered with $\Omega = (0,1) \times (0,1)$ and $\Gamma = \{0\} \times [0,1] \cup [0,1] \times \{0\}$. Injection currents are applied through two electrodes denoted by arrows. The boundary Γ is admissible only for the case (c) and the conductivity is fully recovered. Noise is not added in these examples.

Domain of Dependence and Influence

In the construction algorithm the conductivity of a given cell is obtained after a series of cell by cell computations. In the algorithm the conductivity at a given cell is decided by the cells on its left and below. We call this region the *domain of dependence* of the conductivity at x (see Figure 3.4(a)). Therefore, the noise of current data in this region is the source of the error of the conductivity at x. Similarly, the conductivity value at a give cell propagates to the cells on its right and above. We call this region the *domain of influence* of the information at x (see Figure 3.4(b)).

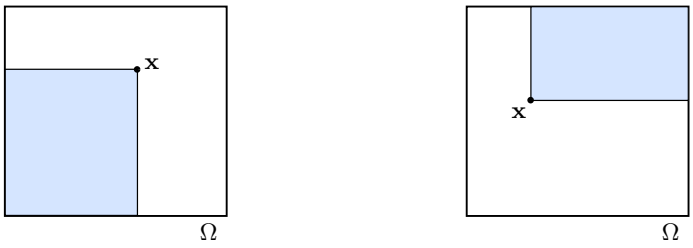

(a) domain of dependence (b) domain of influence

Figure 3.4: The domain of dependence of a conductivity value and the domain of influence of the data at a point $\mathbf{x} \in \Omega$ are in the figures. The show a hyperbolic nature in the curl equation (3.1).

The existence of domains of dependence and influence shows a hyperbolic nature of the problem. In continuum, the domain of dependence and influence for a point is the characteristic line passing the point. A wider region of dependence in our discretization allows a chance to get noises mixed and dissipate. Later we will see that, if the network is parallel to characteristic lines, the domains of dependence and influence becomes a stripe along the characteristic line and the recovered image contains stripes of noises. Hence, it becomes important to design network in a way to avoid such a situation.

Characteristic lines and Noise Propagation along Characteristics

Recall that we may find r by method of characteristic as seen in the formula (2.11) in preceding chapter

$$r(\mathbf{x}(s,t)) = r(\mathbf{x}(s,0)) \exp\left(\int_0^t \nabla \times \mathbf{F}(\mathbf{x}(s,\tau))\, d\tau\right)$$

where $\mathbf{x}(s,0) \in \Gamma \subset \partial\Omega$ and $r(\mathbf{x}(s,0))$ is the given boundary condition.

The curve $\mathbf{x}(s,\cdot)$ is called a *characteristic line*. One can easily see that this curve is an equipotential line for an isotropic conductivity case since the current density $\mathbf{J}$ and the electrical field $\mathbf{E} = -\nabla u$ are parallel to each other.

Remark 3.2.2 (Equipotential line method)**.** *The equipotential lines are easily obtained from* $\mathbf{J}$ *for an isotropic case. Since the voltage* u *is constant on it, one may compute the voltage first if the boundary voltage is given. Then, the conductivity is obtained by Ohm's law. This algorithm is called an equipotential line method (see [11]) (see Figure 3.11).*

Remark 3.2.3 (Direct integration method)**.** *One may use the formula (2.11) to directly compute the resistivity along characteristic lines. Reconstructed conductivity images by such a direct integration are given in Figure 3.12. This is basically the same method used by Ider et al. [15, Figure 6]. If two sets of current data are given, the performance can be improved by integrating along non-characteristic lines even with* 10% *multiplicative noise [15, Figure 4].*

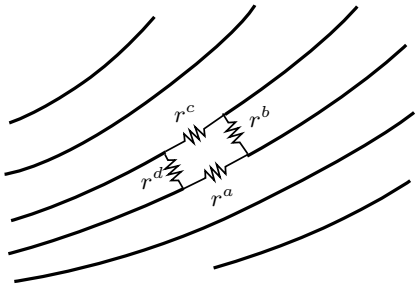

Figure 3.5: VRN and equipotential lines. If VRN is aligned along equipotential lines, the conductivity reconstruction process becomes more sensitive to noise.

Consider a case that the virtual network is aligned along characteristic lines as in Figure 3.5. Then, since there is not electrical current that passes along the equipotential lines, we have $F_a = F_c = 0$. Therefore, Eq. (3.6) becomes

$$r^b F^b - r^d F^d = 0 \quad \text{or} \quad r^b = r^d F^d / F^b.$$

Notice that only the information along the characteristic line is used to compute r^b and hence the domains of dependence and influence are restricted to the cells along the characteristic line. Therefore, the algorithm has no regularizing effect, and VRN becomes like the Direct Integration algorithm. In other words, it is important not to align the virtual network system in a direction which is parallel to the equipotential lines. Rotating a network in the next section is one of the strategies to avoid such a situation locally.

3.2.2 Rotating a VRN

Considering that the posed resistive network is a *virtual*, we may choose the one in arbitrary shape. In this section we consider a technique of rotating network of same rectangular shape. We have two

reasons for the rotation. First, the relation (3.8) is applicable only if $F^b - F^c \ncong 0$. The choice of admissible boundary (see Section 3.2.1) gives a best chance to avoid such a situation. However, if the current datum $\mathbf{F}$ contains a noise, the case of $F^b - F^c \cong 0$ is not avoidable in some regions. By rotating the network we expect noise effects in some region may disappear with a rotation angle. Another reason is to avoid a region that the network is parallel to the characteristic lines. In this way we may reduce the stripes of noises from reconstructed images. Notice that we may produce several conductivity images using a single set of current data if different rotation angles are used. Comparing these images may help us to distinguish the effect of noise and true conductivity (see Remark 3.2.6). It is an important point that this analysis is affordable because the VRN algorithm for a fixed network is solved almost instantly in a ordinary computer. In the following sections the detailed technique of rotating VRN is discussed.

Stream Function

Suppose that a current density $\mathbf{F}$ is given along network edges. If the network is rotated, one should reassign the current density along new edges by interpolating the given data. However, a new noise may appear in doing that and, more importantly, basic physical laws such as Kirchoff's current law can be broken. In this section we develop an interpolation method based on the *stream function* that keeps Kirchoff's current law.

We solve (3.4) to find a *stream function* ψ inside the domain Ω. Let $c = y^{j+1} - y^j = x^{i+1} - x^i$. Then, (3.4) is written as

$$\begin{aligned} cF^{i+\frac{1}{2}\,j} &= \psi^{i+\frac{1}{2}\,j+\frac{1}{2}} - \psi^{i+\frac{1}{2}\,j-\frac{1}{2}}, \quad 0 \le i < n,\ 0 < j < n, \\ -cF^{i\,j+\frac{1}{2}} &= \psi^{i+\frac{1}{2}\,j+\frac{1}{2}} - \psi^{i-\frac{1}{2}\,j+\frac{1}{2}}, \quad 0 < i < n,\ 0 \le j < n \end{aligned} \tag{3.9}$$

(see Figure 3.6). Notice that there are n^2 unknowns of $\psi^{i+\frac{1}{2}\,j+\frac{1}{2}}$ with $0 \le i, j < n$ and $2n(n-1)$ equations in (3.9) and hence the system is over determined. However, the sum of incoming current and outgoing current at a given vertex should be identical in a physically meaningful network, which is called Kirchoff's current law and written as

$$F^{i+\frac{1}{2}\,j} - F^{i-\frac{1}{2}\,j} + F^{i\,j+\frac{1}{2}} - F^{i\,j-\frac{1}{2}} = 0, \quad 0 < i, j < n. \tag{3.10}$$

Since the noised current density may not satisfy this relation, we should do the Helmholtz decomposition for the vector field and take the divergence free part (see Section 3.2.4). Notice that there are $(n-1)^2$ number of interior vertices and hence we have $(n-1)^2$ equations in (3.10). Therefore, the total number of independent equations are

$$2n(n-1) - (n-1)^2 = n^2 - 1.$$

Now there is one extra unknown left, which reflects the fact that the stream function is unique up to adding a constant. Hence we may ground it by using an extra equation $\psi^{\frac{1}{2}\,\frac{1}{2}} = 0$ and decide the stream function uniquely. The value of stream function along the outside of the domain can be solved by using the boundary current density (see Figure 3.6(a)). Notice that there are $4n$ exterior values for the stream function and $4n$ boundary edges. Hence, one can easily obtain them using the relations in (3.9).

Remark 3.2.4. *Notice that (3.9) is the network version of the relation* $\mathbf{F}^\perp = \nabla\psi$ *and (3.10) is the network version of incompressibility* $\nabla \cdot \mathbf{F} = \nabla \times \mathbf{F}^\perp = 0$. *Therefore, the existence of* $\psi^{i+\frac{1}{2}\,j+\frac{1}{2}}$ *is simply the network version of the existence of a potential.*

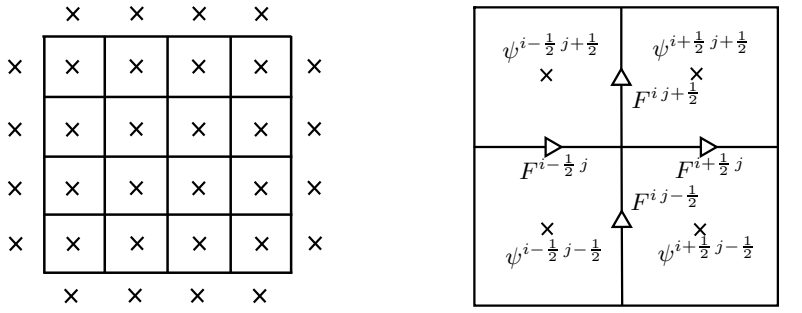

(a) ψ is defined at cell center (b) stream function and current

Figure 3.6: The points marked by $\times$ are where ψ is defined.

Remark 3.2.5 (H^z is the stream function.)**.** *Let* $\mathbf{H}$ *be the magnetic field. Then, the fourth law of Maxwell's equation, or Ampere's law, is written as*

$$\nabla \times \mathbf{H} = \mathbf{J}.$$

In two space dimensions, we have $\partial_z H^y = \partial_z H^x = 0$ *and hence*

$$\begin{pmatrix} J^x \\ J^y \end{pmatrix} = \begin{pmatrix} \partial_y H^z \\ -\partial_x H^z \end{pmatrix},$$

i.e., the stream function is the z-component of the magnetic field. It is the magnetic flux density $\mathbf{B} = \mu\mathbf{H}$ *that is measured by the MRI technology, where the coefficient* μ *is called the permeability. Therefore, for a two dimensional current flow, the mimetic approach in this section is a way to reduce the intermediate data process and to minimise the discretization error.*

Network Rotation

If the stream function for a given current density $\mathbf{F}$ is obtained, one is ready to rotate the network. In Figure 3.7(a) a network system is given before a rotation. In this example, the domain Ω of the conductivity body is the circular disk tangent to the outside square and is placed on the network. In Figure 3.7(b) this network system has been rotated with angle $\theta = 45°$. In that case the edges and the center of each cell represent difference places of the body. Therefore, we should reassign the current data to each of the edges. To do this we first interpolate the values of the stream function at the new centers of rotated cells. Then, the current along each edges is automatically reassigned by the relations in (3.9). In this way we may reduce the discretization error and satisfy Kirchoff's current law.

We will rotate the network for angles with the range of $-20° < \theta < 20°$. Notice that our choice of boundary current is similar to the case of Figure 3.3(c) and hence, if the network is rotated for the angle of $\theta = 45°$, one may obtain an image similar to Figure 3.7(b). If $\theta = 90°$, then the obtained image is similar to Figure 3.7(a). Our purpose is not to find a best angle of rotation, but to distinguish the effect of noise and true conductivity by rotating a network with a relatively small angle. The network rotation gives a series of images for the static conductivity. We may make a movie clip with these static images of different rotation angles. Inconsistent part of the image is the effect of a noise (see Remark 3.2.6). Remember that this movie was made from single set of current data.

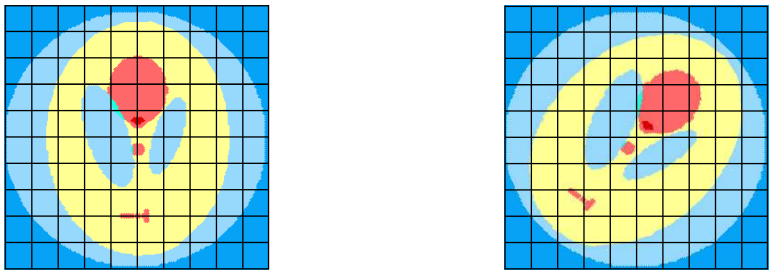

(a) network before rotation $\theta = 0$ (b) rotated body with $\theta = 45^\circ$

Figure 3.7: If a network is rotated, the center of each cell is changed. The value of the stream function at these new cell centers is interpolated. The current density along a new edge is given by these values.

3.2.3 Numerical Simulation Setup

For the numerical simulation we took the target conductivity σ from a Matlab function, which is given in Figure 3.8. This image has been frequently used by many authors. The scale of the conductivity value is

$$0.1 \leq \sigma \leq 0.5.$$

This conductivity corresponds to a resistivity of range $2 \leq r \leq 10$. In the simulation we compute the resistivity distribution first using VRN method and then convert the result in terms of conductivity for easier comparison to other methods. The challenging part of this target conductivity is the discontinuity that may parallel to the electrical current. The physical size of the conductivity body used in the simulation is a disk with a diameter of $50cm$.

The electrical current of $10mA$ was uniformly injected through the circular boundary in the second quadrant, $\frac{\pi}{2} \leq \theta \leq \pi$, where the origin is the center of the circular domain. The same amount of current is uniformly extracted from the boundary in the fourth quadrant, $-\frac{\pi}{2} \leq \theta \leq 0$. The Γ^0 in Definition 2.2.1 consists of these two boundaries. The boundary in the first quadrant, $0 < \theta < \frac{\pi}{2}$, becomes Γ^+ and the one with $-\pi < \theta < -\frac{\pi}{2}$ is Γ^-. For the boundary condition we took $\Gamma = \overline{\Gamma^-}$. This boundary condition can be extended to Γ^0 exactly since the boundary itself is a characteristic line in the region (see [23]).

The current density $\mathbf{J}$ has been obtained by solving a forward problem using a network system, which are displayed in Figure 3.9. It is well known that the network forward solver is equivalent to FDM forward solver (see Strang [36]). The advantage of using network forward solver is to minimize the discretization error. We have obtained a current density $\mathbf{J} = (J^x, J^y)$ with the size of

$$1.1 \times 10^{-3} \ \ [A/m] \leq \ \ |\mathbf{J}| \ \ \leq 4.6 \times 10^{-2} \ \ [A/m].$$

The dimension $[A/m]$ of a current density fits to our two dimensional model. Using the relations in (3.9) and (3.10) we may compute the corresponding stream function ψ. In Figures 3.10(a) and (b), the equipotential lines and the stream lines are given, respectively. The streams lines are level curves of a stream function and perpendicular to equipotential lines.

Multiplicative and Additive Noises

We add a noise to the current data in the following simulations to test the stability of the algorithm. We will add two kinds of noises, which will be called *multiplicative* and *additive* noises. The multiplicative noise of $p\%$ is a random noise computed by

$$\Big(\frac{p}{100}|\mathbf{J}(\mathbf{x})|\Big)\, X,$$

where $-1 \le X \le 1$ is the random variable with a uniform distribution. The size of the multiplicative noise is proportional to the size of current $\mathbf{J}$.

The additive noise follows a normal distribution of average $\mu = 0$ and a standard deviation $s.d. > 0$, say $N(0, s.d.)$. Summing them up gives the current density data used in the simulation which is written as

$$\mathbf{F} = \mathbf{J} + \Big(\frac{p}{100}|\mathbf{J}|\Big)\, X + N(0, s.d.). \tag{3.11}$$

As a measure of additive noise we consider the ratio of signal to standard deviation,

$$S/D := \frac{\text{averaged current } \underline{\text{S}}\text{ignal per edge}}{\text{standard } \underline{\text{D}}\text{eviation of noise}}. \tag{3.12}$$

There are $23,863$ network edges in the interior circular domain and the average current used in the simulation is about $0.078mA$. In the simulation of Figure 3.16 we added an additive noise with a standard deviation $s.d. = 0.003mA$ to each of the edges and hence the ratio is $S/D \cong 26$.

3.2.4 Simulation results

In this section we discuss the simulation results of the VRN method using the current data given in Figure 3.9 and noises in (3.11). This simulation consists of two parts. In the first part, we directly compute using the noised data in (3.11). The VRN method is compared with an equipotential line method (see Remark 3.2.2) and the direct integration (2.11) along characteristic lines (see Remark 3.2.3). In the second part the divergence free part of the Helmholtz decomposition is used. This decomposition process improves the VRN method considerably.

Before Helmholtz Decomposition

The images in Figure 3.11 are reconstructed conductivity distributions obtained by an equipotential line method. We are using the same color map as the one given for the target conductivity in Figure 3.8. From the recovered conductivity images one may observe the stripes along equipotential lines. These show that the noise of current density along the equipotential lines stays in them.

In Figure 3.12 the conductivity images have been reconstructed by the direct integration method given by the formula (2.11). These reconstructed images have the same structure as the ones by the equipotential line method. Notice that equipotential lines and characteristic lines are identical to the isotropic conductivity case and noise inside a characteristic line stays in them. One may say that the performance of these two methods are compatible.

In Figure 3.13, reconstructed conductivity images by the VRN method are given. For the case with 1% multiplicative noise, the conductivity image has been almost recovered. For the case with 5% noise, the strong stripes of the other methods have been disappeared. However, a wide and thin band in the direction of characteristic lines appears. However, one may still observe the small and large anomalies in the domain. A problematic region is the left lower part of the domain. This is a region that the electrical current is parallel to the discontinuity lines of conductivity. Because of that the small anomalies in the

lower middle regions of the domain are not observed. Even if an additive noise is added, the problematic region is the same and the over all picture is similar. Therefore, the remedy for this symptom is obtaining a cleaner data or using a different current data in a different direction. We will see in the next section that the Helmholtz decomposition gives a better chance to resolve this problem.

After Helmholtz Decomposition

The current of a resistive network should satisfy Kirchoff's current law (3.10), which is equivalent to $\nabla \cdot \mathbf{F} = 0$ in a continuous version. However, the current density field $\mathbf{F}$ does not satisfy the relation if a noise is included. In this section we decompose $\mathbf{F}$ into the divergence free and curl free parts using a Helmholtz decomposition algorithm and reconstruct the conductivity image using the divergence free part. Set

$$\mathbf{F} = \begin{pmatrix} \psi_y \\ -\psi_x \end{pmatrix} + \begin{pmatrix} \phi_x \\ \phi_y \end{pmatrix},$$

where the first part is divergence free and the second part is curl free. Therefore,

$$\Delta\psi = -\nabla \times \mathbf{F}, \qquad \Delta\phi = \nabla \cdot \mathbf{F}, \quad x \in \Omega.$$

For the boundary condition, we take

$$\nabla\psi \cdot \mathbf{n}^{\perp} = g, \quad \nabla\phi \cdot \mathbf{n} = \mathbf{F} \cdot \mathbf{n} - g, \quad x \in \partial\Omega.$$

Notice that we only need to find ψ, which is the steam function. The normal component g of boundary current is the one in (1.1), which has been chosen for the experiment but not from measurements.

Conductivity images are reconstructed in Figure 3.14 using the divergence free part of Helmholtz decomposition, where the same 5% multiplicative noise as in the previous section is added. One may find that there is no significant improvement in the equipotential line and direct integration methods. However, the conductivity image reconstructed by the VRN method has been improved considerably. The stripes in the direction of equipotential lines are disappeared. This improvement allows us to increase the noise level considerably when we use the VRN method.

In the next three examples, we test the VRN method with larger noise levels. Three multiplicative noise levels of $10\%, 20\%$ and 30% are tested and the reconstructed conductivity images are given in Figure 3.15. The shapes of larger anomalies are recognizable even with 30% noise. However, smaller ones are not distinguishable if the noise level reaches to 30%. We may observe the stripes parallel to the equipotential lines appeared again if the noise level increases. The reconstructed conductivity images in Figure 3.16 are obtained after adding three additive noises of the signal to standard deviation ratio $S/D = 78, 39$ and 26. One may observe the same phenomenon of noise propagation along the direction of equipotential lines.

Finally, in Figure 3.17, the conductivity images are obtained by the rotated VRN. Three images with three different angles, $\theta = -5, 5$ and 10, are given with an additive noise of $S/D = 39$. The one in the middle of Figure 3.16 is the case with $\theta = 0$. It seems that the effect of true conductivity is more consistent in compare with the effect of a noise under the rotation of the network. It seems that there is no special angle that shows the best image. However, comparing them helps us to distinguish the effect of true conductivity and the noise.

Remark 3.2.6 (Making a Movie Clip)**.** *One may make a movie clip with the conductivity images of several rotation angles. We made a few of them and placed them in " You Tube" with a title of*

"conductivity reconstruction by rotating VRN". Such a movie clip may help us to distinguish the effect of noise and the true conductivity.

3.2.5 Discussion

An isotropic conductivity reconstruction algorithm has been developed in this section when the current density **J** is given in the whole domain. The motivation of this inverse problem is from the magnetic resonance imaging based electrical impedance tomography or simply MREIT. Many authors considered the incompressibility of the current density (1.1) and the Ohm's law to reconstruct the conductivity distribution. However, we have chosen Faraday's law (3.1) since the given current density is directly involved in the equation. Discretization of this curl free equation has been studied relatively less than the divergence free equation. We have constructed a resistive network system to discretize the equation. Then, a contour integration on each cell boundary gives Kirchoff's voltage law. Using this network discretization and the Helmholtz decomposition technique the VRN (virtual resistive network) method suggested in this paper successfully reconstructed the conductivity image. The maximum noise level we have tested is a 30% multiplicative noise or an additive noise of

$$S/D := \frac{\text{averaged current } \underline{\text{S}}\text{ignal per edge}}{\text{standard } \underline{\text{D}}\text{eviation of noise}} \cong 26.$$

The simulation in the paper indicates that the key to a successful conductivity reconstruction is reducing the noise effect that propagates along equipotential lines. Such a trouble is observed from all algorithms including iterative ones (see [22, Figures 1 and 3]). For example, the stripes along equipotential lines ruin the conductivity images by the equipotential line and the direct integration methods even with a low noise level of 1%. The VRN method of this paper shows a robust behavior and we may increase the noise to 30%. However, the stripes still appear as the noise level increases. We may think of two ways to reduce such a noise further. First, one may design various shapes for network system. In this paper we have considered only a network system. However, the network idea has a good flexibility. One may easily construct a triangular network system where Kirchoff's laws of voltage and current can be easily implemented. Rotating a network is also an idea to find an angle with a different (but not necessarily a better) local behavior. Second, one may use another set of current data with different direction of equipotential lines. Then, the noise propagation along characteristic lines can be cancelled to each other. One may also easily distinguish the effect of noise and the true conductivity. In fact, Ider *et al.* used two sets of current data to integrate the term in (2.11) along non-characteristic lines and successfully improved the conductivity image from [15, Figure 6] to [15, Figure 4] with a 10% multiplicative noise. Notice that the VRN method already handles 30% noise using a single set of current data.

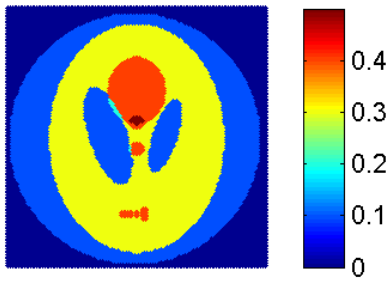

Figure 3.8: True conductivity image used in the simulation. The circular domain tangent to the outside square is used.

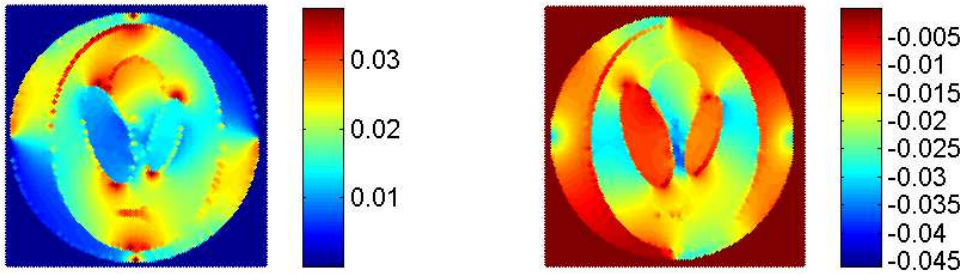

(a) J^x: x-component of current (b) J^y: y-component of current

Figure 3.9: The current $\mathbf{J}$ is obtained by solving the forward problem using 128×128 mesh grids. The number of cells inside the circular domain is 11,934.

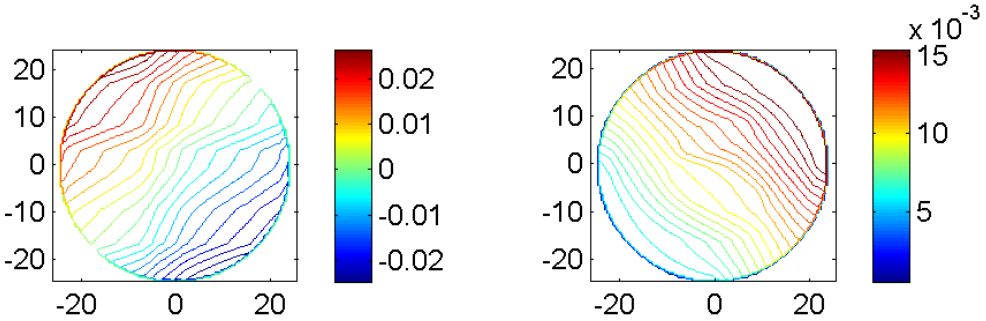

(a) equipotential lines (b) stream lines

Figure 3.10: The equipotential and stream lines of the current density $\mathbf{J}$.

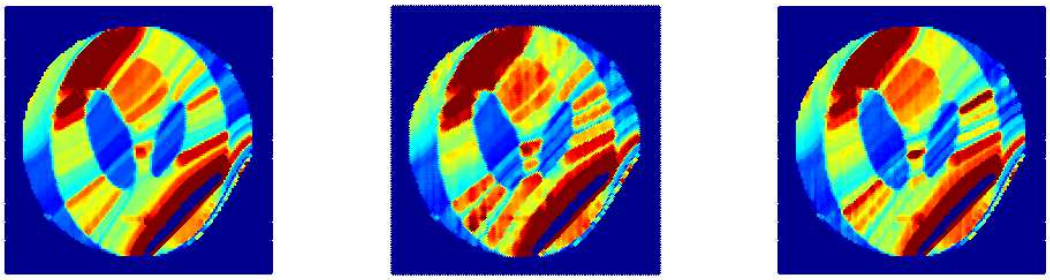

1% multiplicative noise 5% multiplicative noise additive, $S/D = 260$

Figure 3.11: Equipotential line method

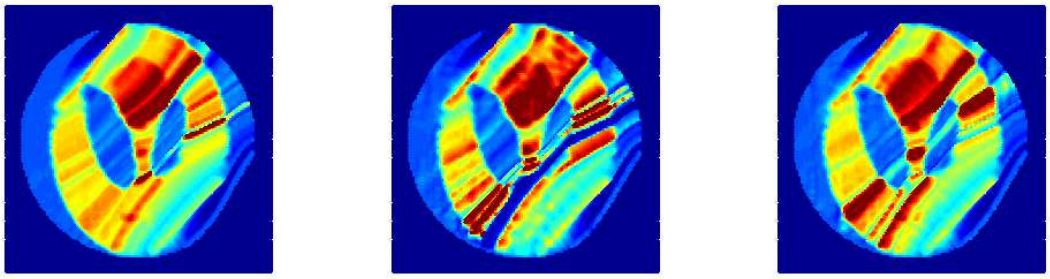

1% multiplicative noise 5% multiplicative noise additive, $S/D = 260$

Figure 3.12: Direct integration given in Eq. (2.11).

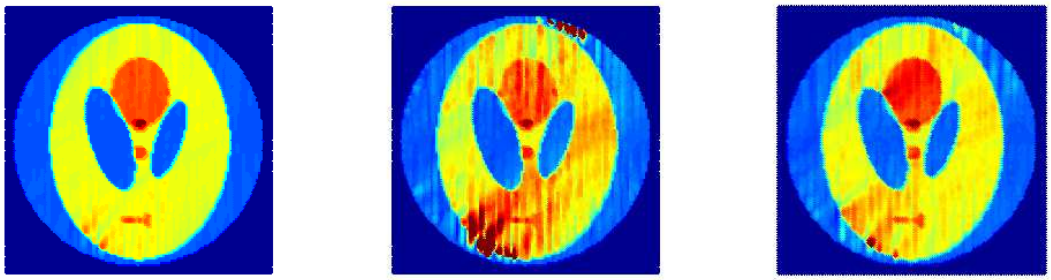

1% multiplicative noise 5% multiplicative noise additive, $S/D = 260$

Figure 3.13: Virtual Resistive Network (VRN)

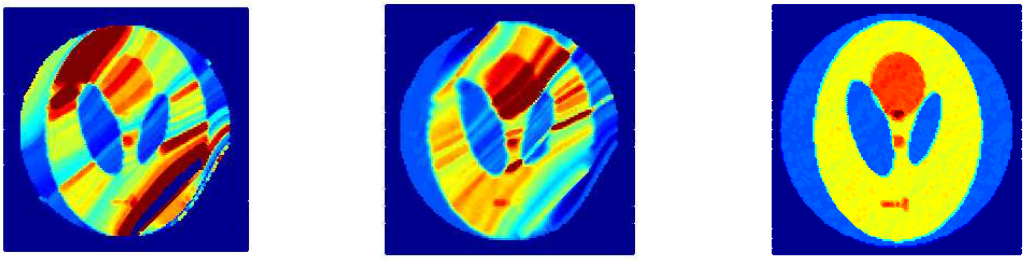

equipotential line direct integration VRN

Figure 3.14: Helmholtz decomposition and a 5% multiplicative noise.

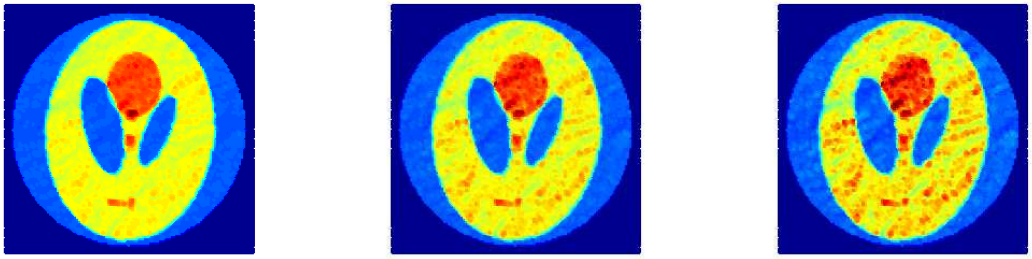

10% 20% 30%

Figure 3.15: VRN with Helmholtz decomposition and multiplicative noises.

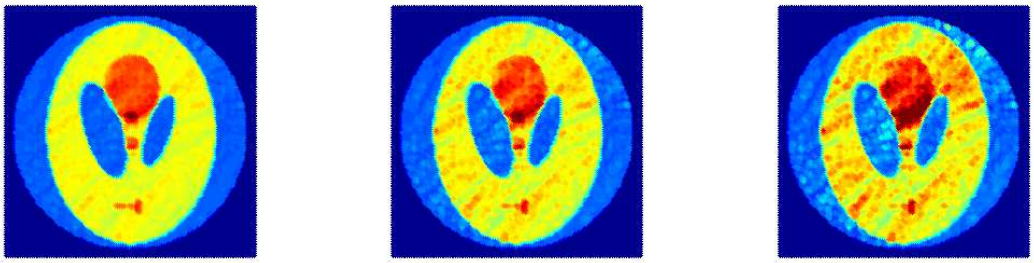

$S/D = 78$ $S/D = 39$ $S/D = 26$

Figure 3.16: VRN with Helmholtz decomposition and additive noises.

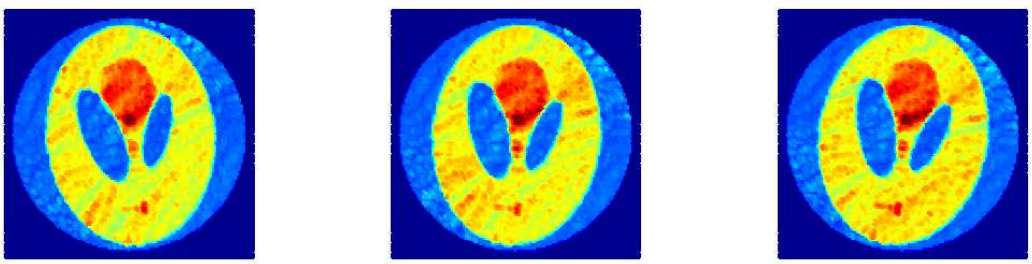

$\theta = -5°$ $\theta = 5°$ $\theta = 10°$

Figure 3.17: Rotated VRN with Helmholtz decomposition ($S/D = 39$).

3.3 Virtual Resistive Network for Orthotropic Materials

Here we apply the VRN algorithm on orthotropic materials. The section is organized in parallel with the preceding section. We first investigate the properties of VRN algorithm on orthotropic problem.

3.3.1 Properties of Rectangular VRN : Orthotropic

We derive a conductivity construction algorithm using a rectangular VRN (virtual resistive network) and investigate its property. We consider a domain $\Omega = (0,1) \times (0,1)$ and the boundary $\Gamma = \{0\} \times [0,1] \cup [0,1] \times \{0\} \subset \partial\Omega$. As was discussed in 3.2.3, there are $(n+1)^2$ vertices, $2n(n+1)$ edges, and n^2 cells. We assume that the boundary resistivity r_0^i is given along the edges on the boundary Γ^i, where Γ^1 is the bottom edges of the network and Γ^2 is the left most edges of the network. (see Figure 3.2(a)). Therefore, $2n$ number of resistors are given initially and therefore, our job is to decide the other $2n^2$ resistors.

As was in 3.2.3, the integration of (3.2) over the area D gives

$$0 = \int_D \nabla \times (r\mathbf{F}) dx = \oint_{\partial D} r\mathbf{F}(z) dz.$$

and we have

$$r^a F_1^a + r^b F_1^b - r^c F_1^c - r^d F_1^d = 0, \tag{3.13}$$

$$r^a F_2^a + r^b F_2^b - r^c F_2^c - r^d F_2^d = 0, \tag{3.14}$$

which is the two Kirchoff's Voltage Laws. Note that there are n^2 number of cells and hence $2n^2$ equations. Therefore those $2n^2$ unknowns can be decided. Note that, the $2n^2 \times 2n^2$ linear system is almost diagonalized. Suppose that two resistors r^a and r^d have been obtained in previous steps or initially. One can find such a cell from Figure 3.2(a), which is at the left bottom corner. From (3.13), (3.14),

$$\begin{pmatrix} r^b \\ r^c \end{pmatrix} = \begin{pmatrix} F_1^b & -F_1^c \\ F_2^b & -F_2^c \end{pmatrix}^{-1} \begin{pmatrix} -r^a F_1^a + r^d F_1^d \\ -r^a F_2^a + r^d F_2^d \end{pmatrix} \tag{3.15}$$

provided

$$F_1^b F_2^c - F_1^c F_2^b \neq 0.$$

Observe the above condition indeed is a discrete version of the admissibility condition for an orthotropic problem (See 2.3.1).

Domain of Dependence and Influence

In the contrary to the isotropic problem, the characteristic lines are not dependent on the data but are always the horizontal and the vertical lines.

For this system, r^1 and r^2, the horizontal and vertical components of resistivity, couple to each other, and their shared domain of dependence are an area enclosed by two characteristic lines and the domain of influence are similar the ones in figure 3.4 (a) and (b). For this case, they are also the ones of continuum hyperbolic system (3.2). However, this coupling is only of the low order one, and in the principal part of the system (3.2) they are decoupled. Hence, the domains of dependence and influence are reduced to a characteristic line when the low order terms can be ignored.

Characteristic lines and Noise Propagation along Characteristics

We encounter the problematic case when the data $\mathbf{F}_1$ and $\mathbf{F}_2$ also are aligned respectively to each family of characteristic lines.

Suppose this happens, for instance $\mathbf{F}_1$ is a horizontal vector field and $\mathbf{F}_2$ is a vertical vector field in a certain region. Then for such a region, the formula (3.15) becomes

$$r_b = -F_d^2/F_b^2\, r_d,$$
$$r_c = -F_a^1/F_c^1\, r_a,$$

and the domain of dependence and influence of a certain horizontal and a vertical resistivity are restricted to a line of edges respectively. Then a noise in a horizontal edge is transported vertically, and a noise in a vertical edge is transported horizontally. These phenomena are indeed observed in simulations as illustrated in Figure 3.18(a) and 3.18(b). We did not put the detailed configuration of this simulation, but we can see from figures vertical stripes and horizontal stripes. The current is injected only through the bottom, and extracted only from the top for the $\mathbf{F}_1$ so that it has the vertical directional tendency, and the current is injected only through the left, and extracted only from the right for the $\mathbf{F}_2$ so that it has the horizontal directional tendency. Therefore, it is desired to design network so that we avoid this

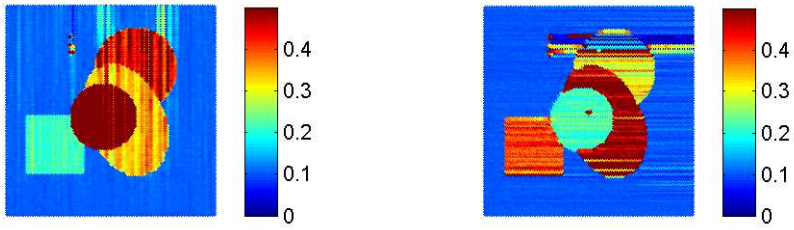

(a) Horizontal component (b) Vertical component

Figure 3.18: The reconstructed image of orthotropic conductivity with $\mathbf{J}_1$ and $\mathbf{J}_2$, where $\mathbf{J}_1$ has a vertical directional tendency, and $\mathbf{J}_2$ has a horizontal directional tendency.

situation.

3.3.2 Mimicking Diagonal Network

One possibility in order to avoid a situation that have the domain of dependence and the domain of influence be restricted on a line, is to consider a network tilted by 45 degree as in Figure 3.19(a). Considering that the characteristic lines are always fixed to be the horizontal and vertical lines, one possible option is to consider a network tilted by 45 degree as in Figure 3.19(a) to have wider domain of dependence and the domain of influence. However, this is to go to another story because we want to obtain the eigenvalues of the resistivity along the horizontal and vertical edges.

One another possibility is still available. Without forgiving the easy implementation of rectangular VRN, one may consider virtual networks of Figure 3.19(b) and 3.19(c). Both of virtual networks are mimicking the tilted network but with cells not tilted. Consider a network of Figure 3.19(b) with two data $\mathbf{F}_1$ and $\mathbf{F}_2$ that are parallel to horizontal lines and vertical lines respectively, which was the case we

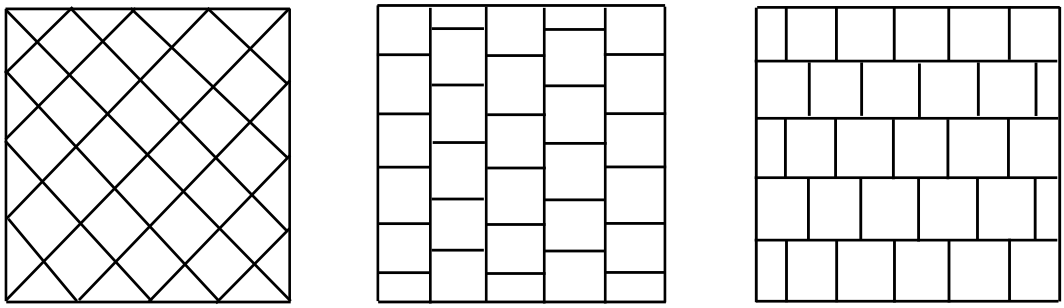

(a) Diagonal disposition of network

(b) Alternate disposition of Horizontal Edges

(c) Alternate disposition of Vertical Edges

Figure 3.19: The two different virtual networks that mimic a diagonal network.

encountered a problem. For this configuration, one verifies that the horizontal resistivity is still depends on and influenced by the vertical line, but the vertical resistivity is now depends on the colored region in the Figure 3.19(b). It is opposite with a configuration of Figure 3.19(c).

Therefore, we reconstruct resistivity twice, one with a network of Figure 3.19(b), and one with a network of Figure 3.19(c), and then pick the vertical values from the former, and the horizontal ones from the latter. Of course, to place the two networks, stream functions of $\mathbf{F}_1$, and $\mathbf{F}_2$ with Helmholtz decomposition are used.

3.3.3 Numerical Simulation Setup

The true conductivity for the orthotropic reconstruction problem is prepared as follows.

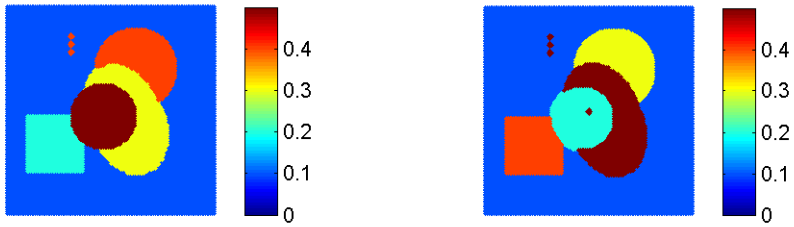

(a) Horizontal eigenvalue

(b) Vertical eigenvaluen

Figure 3.20: True images of horizontal and vertical eigenvalues of conductivity that are used in simulations of orthotropic resistivity reconstruction and simulation setup.

The eigenvalues also have been scaled to be

$$0.1 \leq \sigma_1, \sigma_2 \leq 0.5, \quad \text{or equivalently,} \quad 2 \leq r_1, r_2 \leq 10,$$

where σ_1 and σ_2 are two eigenvalues of conductivity, and r_1 and r_2 are the ones of resistivity.

The physical size of conductivity body used in the simulations was $50cm \times 50cm$. An electrical current of total amount $10mA$ was injected uniformly through the boundary lied in right bottom quadrant assuming the center of body is at origin, and extracted uniformly from the boundary lied in left upper quadrant for the first current data J_1. The same amount through left bottom quadrant and from right upper quadrant for the second data J_2. The locations of injections and extractions are chosen so that the

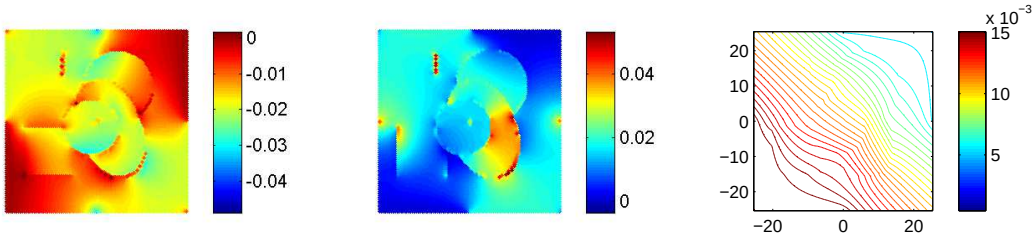

(a) Horizontal component of J_1 (b) Vertical component of J_1 (c) Stream function of J_1

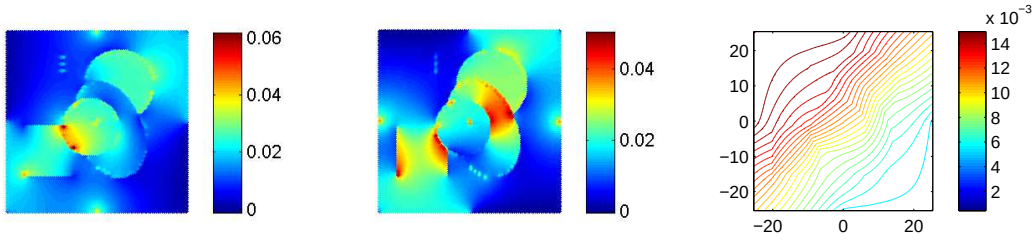

(d) Horizontal component of J_2 (e) Vertical component of J_2 (f) Stream function of J_2

Figure 3.21: Two current data J_1 and J_2 used in simulations of orthotropic resistivity reconstruction.

currents generated do not have tendencies that are aligned with network edges. Also the combination of boundary conditions are the ones that guarantee $\mathbf{J}_1 \times \mathbf{J}_2 \neq 0$. They are illustrated in Figure 3.21.

The sizes of absolute value of data were

$$\begin{aligned} 3.7 \times 10^{-5} \ [A/m^2] \leq \ |J_1| \ \leq 5.3 \times 10^{-2} \ [A/m^2], \\ 1.2 \times 10^{-4} \ [A/m^2] \leq \ |J_2| \ \leq 6.2 \times 10^{-2} \ [A/m^2]. \end{aligned}$$

3.3.4 Simulation Results

In this section we discuss the simulation results of the VRN method using the current data given in Figure 3.21 and noises in (3.11). This simulation consists of two parts. In the first part, we directly compute using the noised data in (3.11). In the second part the divergence free part of the Helmholtz decomposition is used. This decomposition process improves the VRN method considerably.

Before Helmholtz Decomposition

The images in Figure 3.22 are reconstructed conductivity distributions with noised current data. We are using the same color map as the one given for the target conductivity in Figure 3.20. From the recovered conductivity images one may observe the stripes along the vertical and horizontal lines are reduced in compare with images of 3.18(a) and 3.18(b), although we still see them in particular in the figures in the third column. The edges of each regions can be clearly identified. It is very impressive that the small dot in the center of the images of the second row are clearly seen in all of them. The three small dots in the left upper region also are observed as well in all of the figures. However, one also can notice that the noise is still in lower level than what we achieved in the isotropic conductivity reconstruction. Although one cannot compare two reconstruction processes directly, this suggest that it is not sufficient to use the networks mimicking diagonal one, and we are supposed to use Helmholtz decomposition and regularization.

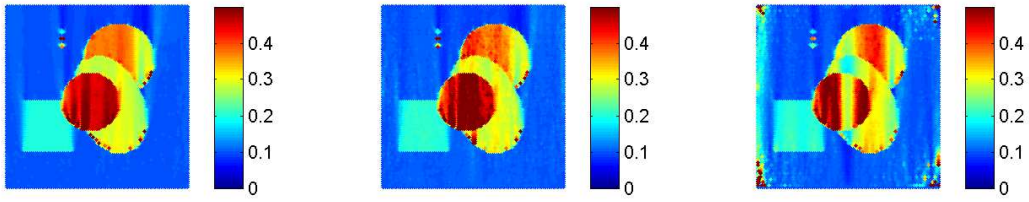

(a) 1% (b) 5% (c) 1%+ additive noise

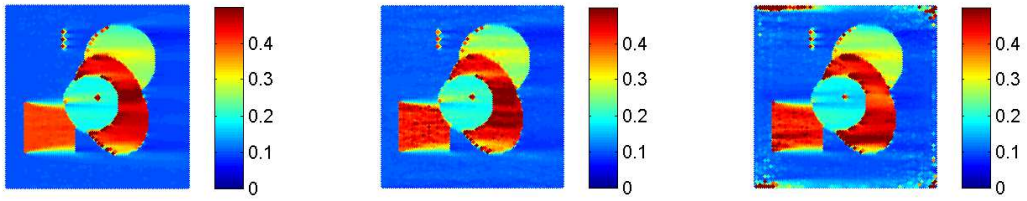

(d) 1% (e) 5% (f) 1%+ additive noise

Figure 3.22: The orthotropic conductivity is reconstructed from J_1 and J_2 that has 1% multiplicative noise, and 5% multiplicative noise, and additive noise with s.d. 0.0003 + multiplicative noise of 1%, respectively. The first row are images of horizontal eigenvalues, and the second row are the ones of vertical eigenvalues.

After Helmholtz Decomposition and Regularization

In this section we decompose $\mathbf{F}_1$ and $\mathbf{F}_2$ into the divergence free and curl free parts respectively using a Helmholtz decomposition algorithm and reconstruct the conductivity image using the divergence free parts as was done in section 3.2.4. Boundary conditions are assigned as same way as in section 3.2.4. After obtaining two stream functions, we performed a regularization by following process. First we set a kernel H_1 by 3×3 matrix

$$\begin{pmatrix} 0.0251 & 0.1453 & 0.0251 \\ 0.1453 & 0.3183 & 0.1453 \\ 0.0251 & 0.1453 & 0.0251 \end{pmatrix}$$

whose entries are summed to 1. The two stream functions are then discrete convoluted by this kernel, which will smooth the data by local averaging. At boundary, the stream functions are extended to have two more columns and two more rows with same values at the boundary so that the convolution can be performed.

Conductivity images are reconstructed in Figure 3.23 using the divergence free parts of Helmholtz decomposition and regularization. We test the VRN method with larger noise levels. Three multiplicative noise levels of 10%, 20% and 30% are tested and the reconstructed conductivity images are given in Figure 3.23. Conductivity values in a certain region are not distinguishable if the noise level reaches to 30%. One can still see the small dot in the center of the images of the second row, and three small dots in the left upper region in all of the figures.

In the next three examples, we added the additive noise with standard deviation 0.0001, 0.0005, and 0.001 respectively. One may find that there is significant improvement.

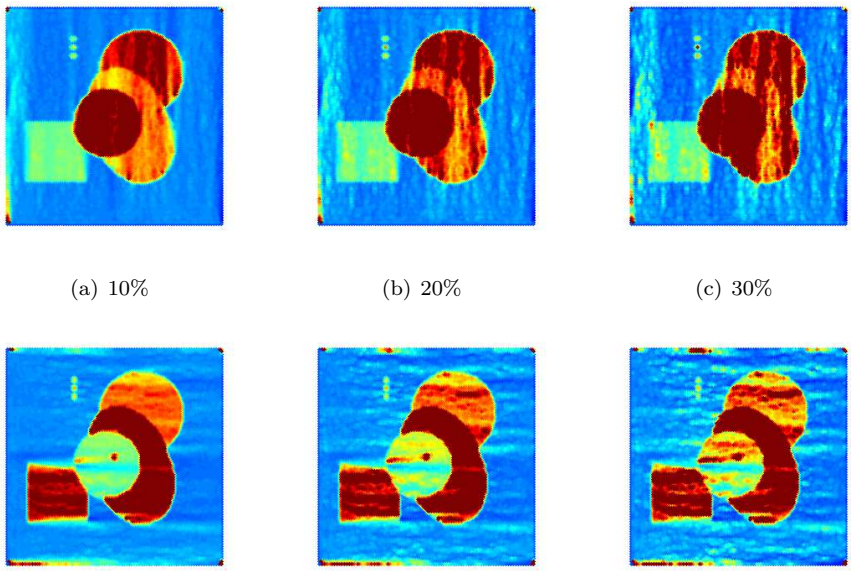

(a) 10% (b) 20% (c) 30%

(d) 10% (e) 20% (f) 30%

Figure 3.23: The orthotropic conductivity is reconstructed from J_1 and J_2 that has 10%, 20%, and 30% multiplicative noise respectively. The first row are images of horizontal eigenvalues, and the second row are the ones of vertical eigenvalues.

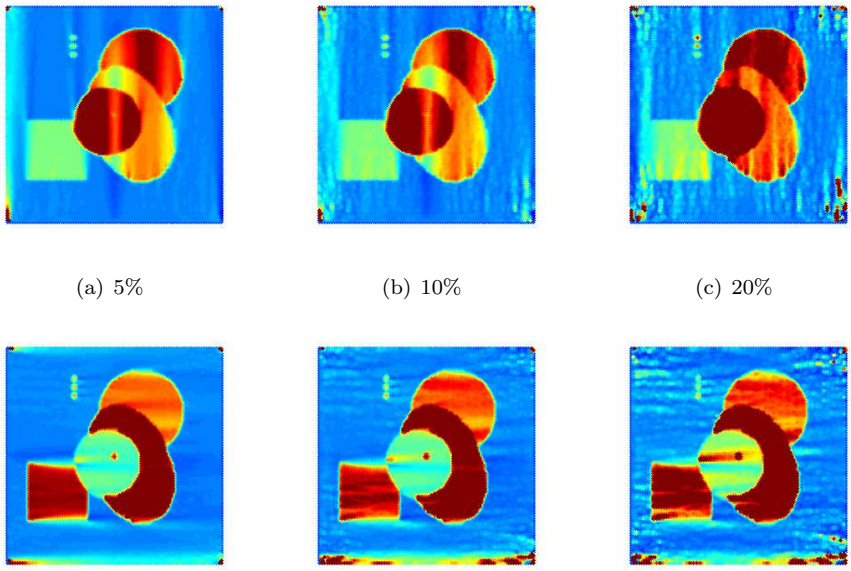

(a) 5% (b) 10% (c) 20%

(d) 5% (e) 10% (f) 20%

Figure 3.24: The orthotropic conductivity is reconstructed from J_1 and J_2 with additive noise with standard deviation 0.0001, 0.0005, and 0.001 respectively. The first row are images of horizontal eigenvalues, and the second row are the ones of vertical eigenvalues.

References

[1] Alberto-P Calderón. On an inverse boundary value problem. In *Seminar on Numerical Analysis and its Applications to Continuum Physics (Rio de Janeiro, 1980)*, page 65–73. Soc. Brasil. Mat., Rio de Janeiro, 1980.

[2] Margaret Cheney, David Isaacson, and Jonathan C. Newell. Electrical impedance tomography. *SIAM Rev.*, 41(1):85–101 (electronic), 1999.

[3] L. Borcea. Electrical impedance tomography. *Inverse problems*, 18:R99, 2002.

[4] Gunther Uhlmann. Recent progress in the anisotropic electrical impedance problem. In *Proceedings of the USA-Chile Workshop on Nonlinear Analysis (Vi na del Mar-Valparaiso, 2000)*, volume 6 of *Electron. J. Differ. Equ. Conf.*, page 303–311 (electronic), San Marcos, TX, 2001. Southwest Texas State Univ.

[5] M Joy, G Scott, and M Henkelman. In vivo detection of applied electric currents by magnetic resonance imaging. *Magnetic resonance imaging*, 7(1):89–94, 1989.

[6] GC Scott, MLG Joy, RL Armstrong, and RM Henkelman. Measurement of nonuniform current density by magnetic resonance. *Medical Imaging, IEEE Transactions on*, 10(3):362–374, 1991.

[7] Nanping Zhang. *Electrical impedance tomography based on current density imaging*. 1992.

[8] Eung Je Woo, Soo Yeol Lee, and Chi Woong Mun. Impedance tomography using internal current density distribution measured by nuclear magnetic resonance. In *Proc. SPIE*, volume 2299, page 377–85, 1994.

[9] Jin Keun Seo, Ohin Kwon, and Eung Je Woo. Magnetic resonance electrical impedance tomography (MREIT): conductivity and current density imaging. In *Journal of Physics: Conference Series*, volume 12, page 140, 2005.

[10] Jin Keun Seo and Eung Je Woo. Magnetic resonance electrical impedance tomography (MREIT). *SIAM Review*, 53(1):40–68, 2011.

[11] Ohin Kwon, June-Yub Lee, and Jeong-Rock Yoon. Equipotential line method for magnetic resonance electrical impedance tomography. *Inverse Problems*, 18(4):1089–1100, 2002.

[12] Ohin Kwon, Eung Je Woo, Jeong-Rock Yoon, and Jin Keun Seo. Magnetic resonance electrical impedance tomography (MREIT): simulation study of j-substitution algorithm. *Biomedical Engineering, IEEE Transactions on*, 49(2):160 –167, February 2002.

[13] Tae Hwi Lee, Hyun Soo Nam, Min Gi Lee, Yong Jung Kim, Eung Je Woo, and Oh In Kwon. Reconstruction of conductivity using the dual-loop method with one injection current in MREIT. *Physics in Medicine and Biology*, 55(24):7523, 2010.

[14] Hyun Soo Nam, Chunjae Park, and Oh In Kwon. Non-iterative conductivity reconstruction algorithm using projected current density in MREIT. *Physics in medicine and biology*, 53(23):6947, 2008.

[15] Y.Z. Ider, S. Onart, and W. Lionheart. Uniqueness and reconstruction in magnetic resonance-electrical impedance tomography (MR-EIT). *Physiological measurement*, 24:591–604, 2003.

[16] Y.Z. Ider and S. Onart. Algebraic reconstruction for 3D magnetic resonance–electrical impedance tomography (MREIT) using one component of magnetic flux density. *Physiological measurement*, 25:281, 2004.

[17] Sungwhan Kim, Ohin Kwon, Jin Keun Seo, and Jeong-Rock Yoon. On a nonlinear partial differential equation arising in magnetic resonance electrical impedance tomography. *SIAM Journal on Mathematical Analysis*, 34(3):511–526 (electronic), 2002.

[18] June-Yub Lee. A reconstruction formula and uniqueness of conductivity in MREIT using two internal current distributions. *Inverse Problems*, 20(3):847–858, 2004.

[19] Adrian Nachman, Alexandru Tamasan, and Alexandre Timonov. Conductivity imaging with a single measurement of boundary and interior data. *Inverse Problems*, 23(6):2551–2563, 2007.

[20] Adrian Nachman, Alexandru Tamasan, and Alexandre Timonov. Recovering the conductivity from a single measurement of interior data. *Inverse Problems*, 25(3):035014, 16, 2009.

[21] Min Gi Lee. Network approach to conductivity recovery. Master's thesis, KAIST, 2009.

[22] Yong Jung Kim, Ohin Kwon, Jin Keun Seo, and Eung Je Woo. Uniqueness and convergence of conductivity image reconstruction in magnetic resonance electrical impedance tomography. *Inverse Problems*, 19(5):1213–1225, 2003.

[23] Yong-Jung Kim and Min-Gi Lee. Well-posedness of the conductivity reconstruction from an interior current density in terms of schauder theory. *To appear in Quart. Appl. Math.*

[24] G. Bal, C. Guo, and F. Monard. Inverse anisotropic conductivity from internal current densities. *ArXiv e-prints*, March 2013.

[25] Giovanni Alessandrini. An identification problem for an elliptic equation in two variables. *Annali di matematica pura ed applicata*, 145(1):265–295, 1986.

[26] Gerard R. Richter. An inverse problem for the steady state diffusion equation. *SIAM Journal on Applied Mathematics*, 41(2):210–221, 1981.

[27] Gerard R. Richter. Numerical identification of a spatially varying diffusion coefficient. *mathematics of computation*, 36(154):375–386, 1981.

[28] G. Bal, E. Bonnetier, F. Monard, and F. Triki. Inverse diffusion from knowledge of power densities. *ArXiv e-prints*, October 2011.

[29] F. Monard and G. Bal. Inverse anisotropic conductivity from power densities in dimension $n \geq 3$. *ArXiv e-prints*, August 2012.

[30] Franccois Monard and Guillaume Bal. Inverse anisotropic diffusion from power density measurements in two dimensions. *Inverse Problems*, 28(8):084001, 20, 2012.

[31] Giovanni Alessandrini. Critical points of solutions of elliptic equations in two variables. *Annali della Scuola Normale Superiore di Pisa. Classe di Scienze. Serie IV*, 14(2):229–256 (1988), 1987.

[32] Earl A. Coddington and Norman Levinson. *Theory of ordinary differential equations*. McGraw-Hill Book Company, Inc., New York-Toronto-London, 1955.

[33] Hermann Weyl. The method of orthogonal projection in potential theory. *Duke Mathematical Journal*, 7:411–444, 1940.

[34] John K. Beem, Paul E. Ehrlich, and Kevin L. Easley. *Global Lorentzian geometry*, volume 202 of *Monographs and Textbooks in Pure and Applied Mathematics*. Marcel Dekker, Inc., New York, second edition, 1996.

[35] G. H. Meisters and C. Olech. Locally one-to-one mappings and a classical theorem on schlicht functions. *Duke Math. J.*, 30:63–80, 1963.

[36] Gilbert Strang. *Introduction to applied mathematics*. Wellesley-Cambridge Press, Wellesley, MA, 1986.

[37] Pavel B. Bochev and James M. Hyman. Principles of mimetic discretizations of differential operators. In *Compatible spatial discretizations*, volume 142 of *IMA Vol. Math. Appl.*, pages 89–119. Springer, New York, 2006.

[38] Douglas N. Arnold, Pavel B. Bochev, Richard B. Lehoucq, Roy A. Nicolaides, and Mikhail Shashkov, editors. *Compatible spatial discretizations*, volume 142 of *The IMA Volumes in Mathematics and its Applications*. Springer, New York, 2006. Papers from the IMA Hot Topics Workshop on Compatible Spatial Discretizations for Partial Differential Equations held at the University of Minnesota, Minneapolis, MN, May 11–15, 2004.

[39] Douglas N. Arnold, Richard S. Falk, and Ragnar Winther. Finite element exterior calculus, homological techniques, and applications. *Acta Numer.*, 15:1–155, 2006.

[40] Douglas N. Arnold, Richard S. Falk, and Ragnar Winther. Finite element exterior calculus: from Hodge theory to numerical stability. *Bull. Amer. Math. Soc. (N.S.)*, 47(2):281–354, 2010.

Summary

Well-posedness in anisotropic conductivity reconstruction

주어진 영역을 흐르는 전류분포를 알때에, 옴의 법칙을 만족하는 전도도를 복구하는 문제를 다룬다. 가장 중요한 결과로서 2차원에서 이방성 전도도에 대한 Well-poseness 정리가 제시된다. 본 문제의 큰 동기가 인체조직의 전도도를 구하고자 하는 것에서 비롯되었고, 인체조직은 특히 이방성 전도도를 띈다는 것을 고려할때에, 이러한 결과는 의의를 가지고 있다 하겠다.

논문의 첫번째 파트에서는 Isotropic, Orthotropic, 그리고 Anisotropic 전도도에 대한 Well-posedness 정리가 제시되어있다. 특히 해의 존재성에 관한 정리를 해의 유일성에 관한 정리만큼 중요하게 다루었다. 해의 존재성을 보장하기 위한 데이터의 충분조건을 위의 정리들과 병행하여 제시한다. 이 조건들은 임의의 벡터필드데이터와 전기적으로 실현가능한 벡터필드데이터의 차이를 특징지우는 하나의 충분조건이 된다. 한편 주요 정리들을 증명하는 것의 핵심단계는 전도도를 미지수로 하는 Hyperbolic 타입의 미분방정식을 세우는 것이다.

논문의 두번째 파트에서는 전도도를 구하는 수치 알고리듬이 제안되어 있다. Isotropic과 Orthotropic 전도도에 대하여 적용할 수 있는 알고리듬이다. 여기서 제안한 알고리듬은 두가지 장점이 두드러진다. 첫번째는 위에서 언급한 Hyperbolic 타입의 미분방정식을 직접 풀어서 전도도를 계산하기 때문에, 반복적 구조를 사용하지 않는다는 점이다. 두번째는 미메틱 방법으로 알려진 이산화과정을 사용하여, div와 curl 오퍼레이터들을 꼭 맞게 이산화된 수준에서 오차없이 계산한다는 점이다. 이러한 이산화에서 얻어진 수치 구조는 회로이론에서 저항네트워크를 구성한 것으로 해석할 수 있기때문에, 우리는 이 알고리듬을 가상저항네트워크 알고리듬이라 부른다. 노이즈의 전파와 알고리듬의 노이즈에 대한 안정성이 탐구된다. 일반적으로 노이즈가 상호 소거되지 않고, characteristic line을 따라 전파되는 것은 Hyperbolic 타입 문제의 본질적 성질이다. 논문에서 사용된 미메틱 방법에 의한 수치구조는 이러한 Hyperbolic 타입 문제의 특징을 완화하는 것으로 나타났다.

감 사 의 글

이 논문을 완성하기까지 주위의 모든 분들로부터 수많은 도움을 받았습니다. 대학원 생활 내내 부족한 저에게 연구자의 자세를 일깨워 주신 김용정 지도교수님께 진심으로 감사드립니다.

대학원 생활을 통하여 한국과학기술원, 한국과학재단, 국방과학연구소, 그리고 한국연구재단에서 많은 지원을 받았습니다.

바쁘신 와중에도 심사에 참여해 주신 변재형 교수님과 임미경 교수님, 그리고 대전까지 참석해 주신 인하대학교 강현배 교수님과 건국대학교 권오인 교수님께 진심으로 감사드립니다. 특히 강현배 교수님, 임미경 교수님, 권오인 교수님께서는 그동안 제가 필요로 할때 도움과 조언을 구할 수 있는 분들이셨습니다. 그리고 방문기간동안 예비심사에 참여해 주신 Habib Ammari 교수님께도 감사드립니다.

매년 방문하셨던 Marshall Slemrod 교수님께는 정말 많은 것을 얻고 배웠습니다. 항상 잊지 않으시고, 저의 연구와 진로가 더욱 확장될 수 있도록에 도움과 조언을 아끼지 않으셨습니다. 마음 속 깊이 감사 드리고 싶습니다.

학과 내에서 학부때부터 저에게 많은 가르침을 주신 이창옥 교수님, 김홍오 교수님, 권길헌 교수님, 황강욱 교수님 덕분에 대학원까지 진학하여 지금까지 흥미를 가지고 공부를 계속 할 수 있었습니다. 진심으로 감사드리고 싶습니다.

대학원생활 중에 인연이 닿았던 모든 분들과의 교류가 저의 가장 큰 대학원 생활이었습니다. 나원상 교수님, 하영수 박사님, 조은주 박사님, 이영란 박사님, 권오상 박사님, 윤석배 박사님께 많은 것을 보고 배웠습니다. 재환씨, 창욱씨, 민수씨와 항상 이야기하고 토론하며 공부를 이어왔습니다. 저에게 자랑인 친구이자 선배, 후배가 되어주었습니다. 웅대와 지은이, 효원씨, 상현씨, 정상근 연구원님과도 많은 일을 함께 할 수 있어서 고마웠습니다. 또 앞서 졸업하여 포닥으로 와있는 선호를 알게되어 기쁘고, 또 많은 도움을 받았습니다. 경림이, 대관이, 제준이, 원상이, 성천이에게도 감사의 인사를 전하고 싶습니다.

끝으로 오늘의 제가 있을 수 있는 것은 모두 어머니와 아버지의 사랑과 보아온 모습들 덕분입니다. 그리고 저의 등대같은 존재였던 형과 가족들에게 감사드립니다. 처가쪽 식구들, 어머님 아버님께 많은 관용과 사랑을 받았습니다. 말이 필요없는, 나의 사랑하는 아내와 두 딸 승혜와 승연이는 저의 일부로서 모든 마음을 함께하고 있습니다.

저의 이 작은 결실이 그분들께 조금이나마 보답이 되기를 바랍니다.

이 력 서

이 름 : 이 민 기

생 년 월 일 : 1981년 9월 2일

E-mail 주 소 : mg.lee@kaist.ac.kr

학 력

1997. 3. – 1999. 2. 한성과학고등학교 (2년 수료)

1999. 3. – 2007. 8. 한국과학기술원 수리과학과 (B.S.), 한국과학기술원 전기 및 전자 공학과 부전공

2007. 9. – 2009. 8. 한국과학기술원 수리과학과 (M.S.)

경 력

2003. 12. – 2005. 12. 대한민국 육군

2010. 3. – 2012. 2. 참여연구원 (한국과학재단사업)

2010. 9. – 2012. 12. 참여연구원 (국방과학연구소사업)

2011. 3. – National Junior Research Fellowship

연 구 업 적

1. **M.-G. Lee**, *Network approach to conductivity recovery*, Master's thesis, KAIST 2009.
2. Y.-J. Kim, and **M.-G. Lee**, *Well-posedness of the conductivity reconstruction from an interior current density in terms of Schauder theory*, to appear in Quart. Appl. Math.
3. T.H. Lee, H.S. Nam, **M.G. Lee**, Y.-J. Kim, E.J. Woo and O.I. Kwon, *Reconstruction of conductivity using dual loop method with one injection current in MREIT*, Phys. Med. Biol., 2010.
4. **M.-G. Lee**, M.-S. Ko, Y.-J. Kim, *Virtual Resistive Network and Conductivity Reconstruction with Faraday's law*, submitted to Inverse Problems.
5. Y.-J. Kim, **M.-G. Lee** and M. Slemrod, *Thermal creep of a rarefied gas on the basis of non-linear Korteweg-theory*, to appear in Archive for Rational Mechanics and Analysis.